12-2015

Estimation of Deep Drainage Differences between Till and No-Till Irrigated Agriculture

Justin P. Gibson
University of Nebraska-Lincoln, j.p.gibson8@gmail.com

Estimation of Deep Drainage Differences between Till and No-till Irrigated Agriculture

by

Justin Philip Gibson

A THESIS

Presented to the Faculty of

The Graduate College at the University of Nebraska

In Partial Fulfillment of Requirements

For the Degree of Master of Science

Major: Earth and Atmospheric Sciences

Under the Supervision of Professor Vitaly A. Zlotnik

Lincoln, Nebraska

December, 2015

Estimation of Deep Drainage Differences between Till and No-Till Irrigated Agriculture

Justin Philip Gibson, M.S.

University of Nebraska, 2015

Adviser: Vitaly A. Zlotnik

Deep drainage was monitored under two center pivot irrigation sites located in south-central Nebraska during the 2013, and part of the 2014, growing seasons. Both fields underwent similar land management except for tillage practice: no-till in one and disk till in the other. Long term deep drainage rates were also estimated from chemical analysis of extracted soil cores, with the aid of the chloride mass balance equation. Mechanisms underpinning differences in deep drainage between the two fields were investigated through the use of unsaturated zone numerical modeling.

Deep drainage estimates from field monitoring indicated that a greater amount of deep drainage occurred in the till field (250 mm/yr) than in the no-till field (50 mm/yr) over the 2013 growing season. In contrast, the chemically based tracer deep drainage estimate indicated more deep drainage in the no-till field (210 mm/yr) than in the till field (100 mm/yr) over the 5 years considered in the analysis. Based on evidence from numerical modeling and water balance estimates, the inference that the tilled site had higher drainage in 2013 but lower drainage averaged over 2008-2013 is attributable to greater irrigation rates at the tilled site in 2013.

Results of the vadose zone modeling suggest that for both tillage practices, deep drainage is primarily occurring in the spring. However, differences in deep drainage rates between the tillage practices occur primarily in the fall. The source of this difference is to be due attributable to irrigation scheduling and differences in evapotranspiration. Results of a vadose zone modeling uncertainty analysis indicate that deep drainage estimation uncertainty is higher with the use of a pedotransfer function as compared to a laboratory measured water retention function. Additionally, it was found that the sensitivity of deep drainage rates to van Genuchten water retention fitting parameters (specifically α and n) changes between different irrigation application regimes.

Acknowledgements

Completion of this research would not have been possible without funding support from the Nebraska Environmental Trust, whose dedication to the conservation of Nebraska's natural environments ensures a positive future for our great state. The opportunity for a research assistantship was instrumental in my completion of this project.

First and foremost, I would like to thank my mentor, Dr. John Gates. Dr. Gates has been the most influential person in my academic career, having instilled in me a passion for natural science and hydrogeology. He has given me invaluable skills and experience that I will take with me as I pursue a professional career, and it was an honor to learn from him.

I would like to thank my committee members: Dr. Vitaly Zlotnik, Dr. Suat Irmak, Dr. Dean Eisenhauer, and Dr. Darryll Pederson for their continual insight, advice, and support. Special thanks go to Dr. Suat Irmak for project initiation, funding, and leadership. Dr. Zlotnik, in particular, has been a great help in facilitating my completion of this project.

Support and input from Dr. Larry Murdoch, Dr. Trenton Franz, and Dr. Patricio Grassini in the form of equipment, expertise, and data was greatly appreciated and enabled me to more thoroughly complete my research.

Lastly, a special thanks to my friends and family for their encouragement, love, and guidance throughout my academic career.

Table of Contents

Abstract

Acknowledgements

Table of Contents

Table of Figures

Table of Tables

List of Parameters and Abbreviations

1 Chapter 1: Introduction 1

2 Chapter 2: Assessing the Impact of Tillage on Deep Drainage with Physical and Chemical Estimation Methods 5

2.1 Introduction 5

2.2 Study Area 5

2.3 Methods for Deep Drainage Estimations 6

2.3.1 Soil Core Analysis 6

2.3.2 Chloride Mass Balance 8

2.3.3 Lysimetry 13

2.3.4 Water Retention Functions 14

2.3.5 Buckingham-Darcy 14

2.4 Results and Discussion of Deep Drainage Estimations 16

2.4.1 Soil Core Analysis 16

2.4.2 Chloride Mass Balance 19

2.4.3 Lysimetry 25

2.4.4 Water Retention Functions 30

2.4.5 Buckingham-Darcy 31

2.4.6 Comparison of Previous Deep Drainage Estimates 34

2.5 Summary and Conclusions 35

3 Chapter 3: Assessing the Mechanisms Leading to Differences in Deep Drainage Rates Under Irrigated Till and No-till Agriculture with Unsaturated Zone Numerical Modeling 37

3.1 Introduction 37

3.2 Methods of Numerical Modeling 39

3.2.1 Vadose Zone Model 39
3.2.2 Weather Data 39
3.2.3 Estimating Potential Evapotranspiration 39
3.2.4 Irrigation Regimes 41
3.2.5 Soil Profile Information 43
3.2.6 Coupling of HYDRUS 1D and MATLAB 43
3.2.7 Error Sources in Vadose Zone Modeling 44
3.2.8 Monte Carlo Probabilistic Error Analysis 46
3.3 Results and Discussion of Simulations 48
3.3.1 Timing and Magnitudes of Deep Drainage: Till vs No-till 48
3.3.2 ET_a Difference: Till vs. No-till 49
3.3.3 Irrigation Application 56
3.3.4 Uncertainty Analysis 59
3.3.4.1 Impact of Irrigation Regime 59
3.3.4.2 LM vs PTF for Water Retention Functions 59
3.3.4.3 Model Parameter Correlation with Deep Drainage Rates 62
3.3.4.4 Parameter α 66
3.3.4.5 Parameter n 68
3.3.4.6 Maximum Rooting Depth Parameter 69
3.4 Summary and Conclusions 70
4 Chapter 4: Conclusions 72
References 74
Appendix A: Monte Carlo Uncertainty Analysis 79
Appendix B: Geophysical Survey 80
Appendix C: Extensometer Sensors 82
Appendix D: Estimating Evapotranspiration for the No-till Field 86

Table of Figures

Figure 2.1: Study Location located southeast of Holdrege, NE.

Figure 2.2: Assuming an approximate 26,000 mg/m^2 of Cl^- was applied from precipitation and irrigation over 2008-2012, the depth of deep drainage water from 2008 to 2012 would be 5 m (dashed line). Deep drainage water is calculated as depth-integrated water content over this interval. (Figure adapted from Healy, 2010).

Figure 2.3: No-till field extracted core gravimetric moisture (u), and Cl^- profiles.

Figure 2.4: Till field extracted core gravimetric moisture (u), and Cl^- profiles.

Figure 2.5: Annual irrigation application for both the till and no-till fields as measured by the in-field NRD flow meters.

Figure 2.6 Cumulative distribution function (CDF) for CMB MC deep drainage calculations representing average deep drainage over 5 years for the A) till and B) no-till field. Red lines indicate mean values of deep drainage.

Figure 2.7: Probability density function (PDF) of average deep drainage rates calculated from the CMB equation with averaged soil moisture, and averaged Cl^- concentration profiles for each field. Red lines indicate mean deep drainage rates.

Figure 2.8: Probability density function (PDF) of average deep drainage rates calculated from the CMB equation over the period of 2005-2013 with averaged soil moisture, and averaged Cl^- concentration profiles for each field. Red lines indicate mean deep drainage rates.

Figure 2.9: Deep drainage in the A) till field and B) no-till field over the 2013 growing season as measured by the lysimeters. Note that the in the till field (A), time between each drainage peak is about 3-4 days. This time lag is similar to the time the center pivot needs to move around the entire field.

Figure 2.10: Cumulative precipitation, irrigation, and drainage over the 2013 growing season for the A) till and B) no-till fields.

Figure 2.11: Qualitative analysis of both irrigation and precipitation events and their corresponding drainage events.

Figure 2.12: Water retention curves for soil samples measured in lab.

Figure 2.13 A) till and B) no-till field pressure head (h) time series for the 2013 growing season.

Figure 2.14: Cumulative precipitation, irrigation, and deep drainage (DD) measured by a lysimeter and from Buckingham-Darcy.

Figure 2.15: Probability density function (PDF) of deep drainage as calculated by the MC analysis for the Buckingham-Darcy method. The upward (negative) drainage in the no-till field may be due to a sensor malfunction. Red lines indicate mean deep drainage rates.

Figure 3.1: 11-year simulation results split into annual cumulative time series for the major water balance components (precipitation, ET_a, irrigation, and deep drainage) in the till field under the pressure head triggered irrigation regime (IR_h).

Figure 3.2: 11-year simulation results split into annual cumulative time series for the major water balance components (precipitation, ET_a, irrigation, and deep drainage) in the till field under the precipitation delayed irrigation regime (IR_{PD}).

Figure 3.3: 11-year simulation results split into annual cumulative time series for the major water balance components (precipitation, ET_a, irrigation, and deep drainage) in the no-till field under the pressure head triggered irrigation regime (IR_h).

Figure 3.4: 11-year simulation results split into annual cumulative time series for the major water balance components (precipitation, ET_a, irrigation, and deep drainage) in the no-till field under the precipitation delayed irrigation regime (IR_{PD}).

Figure 3.5: Annual cumulative deep drainage time series overlain for all years for the till and no-till fields under both irrigation regimes: pressure head triggered (IR_h) and precipitation delayed irrigation (IR_{PD}).

Figure 3.6 Comparison of irrigation application for the A) till and B) no-till fields as measured by the in-field NRD flow meter and estimated by the pressure head triggered irrigation regime (IR_h).

Figure 3.7 Comparison of irrigation application for the A) till and B) no-till fields as measured by the in-field NRD flow meter and estimated by the precipitation delayed irrigation regime (IR_{PD}).

Figure 3.8 Cumulative density function (CDF) for deep drainage under A) pressure head triggered irrigation regime (IR_h) and B) precipitation delayed irrigation regime (IR_{PD}), and two different methods of measuring WRF functions, laboratory measured (LM) and pedotransfer function (PTF). Red lines indicate average deep drainage rates.

Figure 3.9 Unsaturated hydraulic conductivity (K(*h*)) determined by two methods: laboratory measured (LM) and pedotransfer function (PTF) for the A) upper and B) lower soil layers simulated.

Figure 3.10: Correlation between each parameter and 11-year average drainage within the pressure head triggered irrigation regime (IR_h). The top row presents the laboratory measured (LM) WRF parameters and the bottom row presents the pedotransfer function (PTF) WRF parameters.

Figure 3.11: Correlation between each parameter and 11-year average deep drainage within the precipitation delayed irrigation regime (IR_{PD}). The top row presents the laboratory measured (LM) WRF parameters and the bottom row presents the pedotransfer function (PTF) WRF parameters.

Figure 3.12: Hypothetical moisture profile (θ) and corresponding pressure head profile (*h*). With different α values (.003, .005, and .008 (1/cm)), the same water content leads to different pressure head values. The three α values used in this example represent the approximate error range of values for the UL PTF WRF.

Figure 3.13: Correlation between the α parameter for the lower soil layer, average simulated irrigation application, and resulting average deep drainage as simulated under the IR_h with a water retention function determined via pedotransfer function.

Figure 3.14: With different α values, K(*h*) has a wide range for a given pressure head (*h*). The three α values used in this example (.003, .005, .008 (1/cm)) represent the error range of α determined for the UL soil material via PTF.

Figure 3.15: Hypothetical moisture profile (θ) and corresponding pressure head (*h*) profile. With different *n* values (1.5, 1.66, and 1.8 (-)), the same water content leads to different pressure head values. In the wet range, this is not a significant effect.

Figure A.1: Probability density function (PDF) of 2 hypothetical deep drainage outputs from 2 different estimation methods.

Figure B.1: Geophysical survey conducted on the no-till field in early May 2014. Soil water sensors used in the field monitoring experiment were located in the center of the survey.

Figure C.1: Average daily outputs from the extensometer sensors in the no-till field. Lines fit through the data represent a temperature effect.

Figure C.2: Corrected average daily outputs from the extensometer sensors in the no-till field.

Figure C.3: Annotated extensometer time series for the 18’ extensometer with overlain cumulative deep drainage from a nearby lysimeter.

Figure D.1: K_c curve calculated from measured ET_a data at a no-till center pivot irrigation Ameriflux (AF) research site in Mead, NE, and HPRCC published K_c coefficients for corn plotted for reference.

Figure D.2: Time series comparison of measured and predicted ET_a for the Ameriflux Mead, NE, no-till research site.

Table of Tables

Table 2.1: Parameter error ranges used in the CMB Monte Carlo Analysis.

Table 2.2: Average *u*(-) and Cl^- (ppm) for each extracted core.

Table 2.3: Annual irrigation application as reported by in-field flow meters.

Table 2.4: Precipitation, irrigation and Cl^- concentrations used in the CMB equation.

Table 2.5: 5 and 8 year average CMB deep drainage estimates for averaged cores and corresponding values of precipitation and irrigation.

Table 2.6: Irrigation application (mm) in each field for the 2013 growing season as reported by the in-field rain gauge.

Table 2.7 Van Genuchten fitting parameters for soil samples measured in lab.

Table 3.1: Framework of the MC uncertainty analysis with mean values and standard deviations for each input parameter.

Table 3.2 Summary of water balance components from the H1D simulations.

Table 3.3: R^2 and RMSE values for each parameter vs. 11-year average deep drainage rates.

List of Parameters and Abbreviations

Parameter/ abbreviation	Description
(-)	Dimensionless units
CDF	Cumulative distribution function
CHE	Chloride harvest export
CMB	Chloride mass balance
h	Pressure head (-cm)
IDW	Inverse distance weighted
IR_h	Pressure head triggered irrigation regime
IR_{PD}	Precipitation delayed irrigation regime
K(h)	Unsaturated hydraulic conductivity (cm/day)
K_s	Saturated hydraulic conductivity (cm/day)
LM	Laboratory measured
m	Fitting parameter in the van Genuchten water retention equation (-)
MC	Monte Carlo uncertainty analysis
MRD	Maximum rooting depth parameter (cm)
n	Fitting parameter in the van Genuchten water retention equation (-)
PDF	Probability density function
PTF	Pedotransfer function
q	Flux of deep drainage (cm/day)
u	Gravimetric water content (-)
WRF	Water retention function
α	Fitting parameter in the van Genuchten water retention equation (1/cm)
θ	Volumetric water content (-)
θ_r	Residual water content (-)
θ_s	Saturated water content (-)

Chapter 1: Introduction

Groundwater is a vital source of freshwater in Nebraska, representing an important component of the state's economy and daily lives of its people. Nebraska ranks 1st nationally in irrigated acres at 8.3 million acres (USDA, 2014). Of the irrigation water used within the state, 84% comes from groundwater sources (USGS, 2005). To ensure the long-term sustainability of those groundwater sources, a balance must be struck between pumping and groundwater recharge. In order to determine the relative magnitudes of both pumping and recharge, studies frequently measure the difference between them by determining the change in groundwater level (Young et al., 2013). However, this balance occurs over a large spatial scale, and often with a significant lag between the surface and the aquifer. The questions investigated in this study occur on a field scale and are investigated over a relatively short period of time. In this case pumping rates are known and because of this, the focus will be on estimating the remaining component – groundwater recharge – through the use of field scale techniques.

Groundwater recharge is defined as the downward flow of water reaching the water table, adding to groundwater storage (Healy, 2010). Deep drainage is defined as the downward flow of water moving past the base of the root zone (Gates et al., 2014). Within this analysis, deep drainage rates will serve as a proxy for groundwater recharge rates as it is assumed that deep drainage will eventually contribute to recharge after transmission through the unsaturated zone.

Estimations of groundwater recharge have been completed within Nebraska, each highlighting certain environments or hydrogeological systems. Szilagyi et al. (2011)

estimated recharge rates within the Nebraska Sandhills, which comprise approximately 1/3rd of the area of the state. Gates et al. (2014) estimated groundwater recharge in the eastern part of Nebraska and explored the impact of lithological influences of glaciation. However, few studies have focused on estimating recharge under irrigated agriculture, which makes up a significant area of the state – approximately 16% is irrigated cropland (USDA, 2013). While Szilagyi and Jozsa (2013) estimated net recharge rates for the entire state, the study did not consider irrigation application, and as a result did not ascertain the effect of irrigation return flow. This is an important component for considering the potential transport of agricultural additives (Klocke et al., 1999; Spalding et al., 2001; Exner et al., 2014), infiltrated contaminants, and understanding the water balance as a whole. Additionally, the scale at which the water balance was computed (1 km) makes it difficult to discern differences in recharge rates due to variations in land use on the field to sub-field scale.

Previous studies have demonstrated that land use can impact rates of deep drainage (Gates et al., 2011). However, there have been few studies regarding how land management decisions within a single land use can effect rates of deep drainage (Byre et al., 2000; Scanlon et al., 2008). Understanding the influence of land management is important as it presents an opportunity for land users to make decisions that impact the water balance in a direct and purposeful way. This hydrogeological investigation was performed to understand the net effects of land management decisions, specifically tillage practice, within a single land use category (irrigated agriculture), on deep drainage.

Two tillage practices were considered in the study: disk till and no-till. Disk till is defined as using a tandem disk harrow once in the fall, and then using a field cultivator in

the spring before planting (CropWatch, 2014). In a no-till field, tillage is eliminated and weed control is conducted with the use of herbicides. Hydrological benefits of no-till include: an increase in soil organic matter quality (Arshad et al., 1990), resulting in an increase in soil structure (Brady and Weil, 2004) that leads to an increase in saturated hydraulic conductivity (Deck, 2010). An additional benefit from surface residue cover is a decrease in soil water evaporation (Klocke et al., 2009; Odhiambo and Irmak, 2010).

Deep drainage can be estimated experimentally or through the use of a vadose zone model. Experimental studies can be both expensive and time-intensive as multiple methods are often employed in an effort to avoid bias that is specific to each method imposed (Gates et al., 2014; Scanlon, 2008). For this reason modeling tends to be a popular approach, however model parameter error often introduces significant uncertainty into model outputs (Wang et al., 2009).

Primary goals of this study are as follows:

- Use multiple deep drainage estimation techniques (physical direct, physical indirect, and chemical tracer) to experimentally measure the difference in deep drainage rates occurring in two fields with different tillage practices (till and no-till).
- Contextualize the results of each deep drainage estimation method with an uncertainty analysis where applicable.
- Use vadose zone modeling to investigate the mechanisms underpinning differences in deep drainage rates between the till and no-till field.
- Contextualize the results of the vadose zone modeling with an uncertainty analysis that considers: 2 irrigation application methods, 2 methods to obtain

water retention function fitting parameters, and 3 input parameters believed to be sensitive.

We will use two primary groups of experimental deep drainage estimation: physically-based monitoring and tracer tracking methods. Physical methods can be partitioned into direct and indirect measurement. Direct measurement is carried out through the use of an installed device known as a lysimeter. Lysimetry works in principle by intercepting percolating infiltrated water and then quantifying it – often with a tipping bucket mechanism (Gee et al., 2002). Indirect methods infer water motion from measurements of physical properties of soil, and fine-scale temporal measurements of the hydraulic gradients below the root zone. Tracer methods work by tracking a unique time-specific signature of infiltrated water, where typically heat or chemistry serves as the marker (Healy, 2010).

Chapter 2: Assessing the Impact of Tillage on Deep Drainage with Physical and Chemical Estimation Methods

2.1 Introduction

The objective of the in-field monitoring and chemical tracer analysis presented in this chapter is to experimentally assess the impact of two tillage practices on deep drainage occurring under irrigated agriculture. In order to carry this analysis out, two paired experimental fields were studied in south-central Nebraska. Both fields underwent similar land management except for tillage practices: no-till in one and disk till in the other. Multiple methods to estimate deep drainage were utilized in order to avoid bias associated with each method. Deep drainage estimates are presented for each method and, additionally, the impact of analytical error associated with each method (where applicable) on deep drainage was explored through the use of a probabilistic uncertainty analysis.

Deep drainage was monitored over the growing seasons during 2013 and 2014, under a corn/soybean rotation with the soybean season being cut short due to hail damage. In each field, three soil cores were extracted with the use of a direct-push Geoprobe®. Soil-water sensors were installed shortly after planting in the first year and left in place until the conclusion of the experiment. Data obtained from this experiment will be called upon in the subsequent chapter in order to investigate the source of differences in deep drainage between the two fields, with the use of vadose zone modeling.

2.2 Field/Study Area Description

The two experimental fields were located southwest of Holdrege, NE, and approximately ½ mile from each other. The 10 year average precipitation is 590 mm/yr as

reported by a High Plains Regional Climate Center (HPRCC) weather station located 3 miles away. The soil texture in both fields is a Holdrege silt loam with a measured slope of 0.4% (Deck, 2010). Both fields were under center pivot irrigation and paired to match each other in planting date, row direction, planting density, and corn/soybean hybrid.

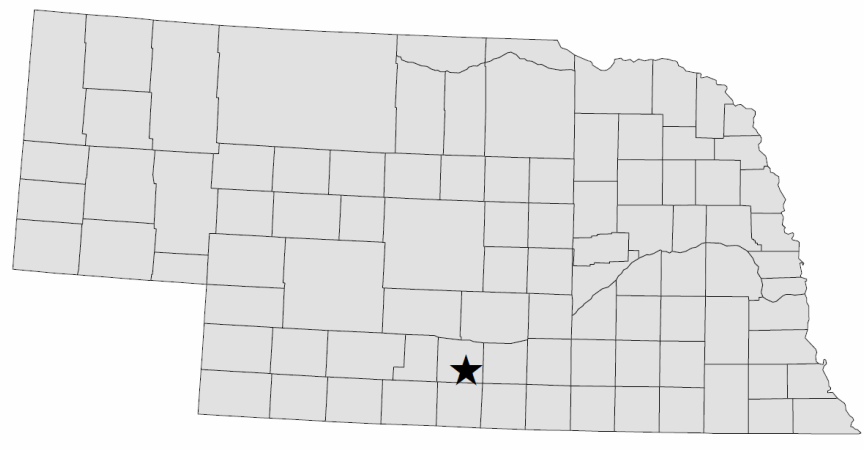

Figure 2.1: Study Location located southeast of Holdrege, NE.

2.3 Methods

In both the no-till and till fields, a similar suite of soil-water sensors were installed that recorded measurements on a sub-hourly scale. Soil pressure head sensors (Watermark™) were installed at 2.4 and 2.7 m depths. A lysimeter (Decagon Draingauge G3™) was installed at a depth of 3 m. In addition to the soil-water sensors, a rain gauge was installed in each field, as well as one on the outside of each field for the purpose of tracking precipitation and irrigation application.

2.3.1 Soil Core Analysis

In both experimental fields, three soil cores were extracted with a direct-push Geoprobe®. The cores were extracted in a line with 10 m spacing in between each extraction point. Central cores were extracted to a depth of 15 m in the till field, and only

to 12 m in the no-till field due to technical limitations of the Geoprobe®. Outer cores were extracted to 7.6 m and in all cases, the extracted cores were cut to a length of 30 cm and stored in a freezer until analysis was performed.

Each soil core was sampled in 30 cm intervals where gravimetric water content and pore water anion concentrations were determined in the lab. Gravimetric water content was measured by weighing samples on a precision balance before and after drying in an oven at 100^{o}C for 24 hours. Anion concentrations were determined by first extracting pore water following the elutriation method of adding deionized water and shaking for 6 hours. After shaking, the samples were spun in a centrifuge for 10 minutes to settle suspended particles. Diluted pore water was then filtered by pushing through a 20 µm filter. Filtered water samples were run through a Dionex™ ion chromatography system and diluted anion concentrations were determined. Because deionized water was added to samples as part of the elutriation process, pore water prior to dilution was back-calculated in order to determine *in situ* concentration. This back-calculation was carried out through the use of the following dilution equation:

$$M_1 = \frac{M_2 V_2}{V_1} \tag{1}$$

where, M_1 is *in situ* pore water concentration (prior to laboratory dilution) (ppm), V_1 is gravimetric water content multiplied by the soil sample mass (g), M_2 is measured concentration of diluted pore water (ppm), and V_2 is the sum of added deionized water used in the analysis and V_1 (g).

2.3.2 Chloride Mass Balance

The use of chloride as an environmental tracer has been carried out in numerous recharge estimation studies (Allison and Hughes, 1983). It is an attractive tracer due to being relatively inexpensive to analyze, as well as naturally occurring in precipitation and irrigation water. Because chloride moves through the subsurface in a conservative manner (Allison and Hughes, 1978), the age of moisture in the vadose zone can be bracketed by comparing cumulative inputs at the surface, with cumulative Cl^- concentrations at depth. The consideration of chloride from irrigation water has been carried out in numerous studies (Lin et al, 2013, Liao, 2012). Assumptions of this method include negligible runoff, run-on, dry deposition, and percolation of infiltrated water is vertical.

In order to provide a deep drainage estimate that is consistent with the timescales of available land use history in this study, care must be taken to ensure that the depth of pore water, or more precisely the age of that pore water, used in the chloride mass balance calculation does not exceed the period of land use history that is available. In this case, records are only available for the years of 2008-2013. Prior to that period, it is uncertain whether different crop rotations or irrigation application methods were used.

The following equation can be applied to profile data in the unsaturated zone to determine the cumulative mass of Cl^- at depth from extracted core samples:

$$\sum Cl^- = \sum_{i=1}^{n} \Delta z_i \, \theta_i \, Cl^-_i \qquad (2)$$

where i begins at the surface sample, n is sample number at the bottom of the core, Δz indicates the length of the sample interval (mm), θ is volumetric water content (-), and Cl^- is chloride concentration in pore water (mg/L).

Similarly, the mass of chloride deposition to the top of the profile can be estimated from the sum of contributions from rainfall and irrigation if it can be assumed that other factors (such as runoff, run-on, and dry deposition) are negligible with the following equation:

$$Cl^{-}_{\text{applied}} = I \cdot c_i + P \cdot c_p \quad (3)$$

where, I is total irrigation application over the study period (mm), c_i is the concentration of Cl^- in irrigation water (mg/L), P is equal to total precipitation over the study period (mm), and c_p is the concentration of Cl^- in rainwater (mg/L).

Using these approaches, it is possible to estimate the elapsed time since infiltration of water at any depth along the profile. Then, deep drainage rate (mm/yr) is calculated as the depth-integrated volumetric water content from the surface to the depth where Cl^-_{applied} is equal to $\sum Cl^-$ at depth (Fig 2.2):

$$Deep\ Drainage = \sum_{i=1}^{n} \Delta z_i \theta_i \quad (4)$$

where i begins at the surface sample, Δz indicates the length of the sample interval (mm), and θ is volumetric water content (-).

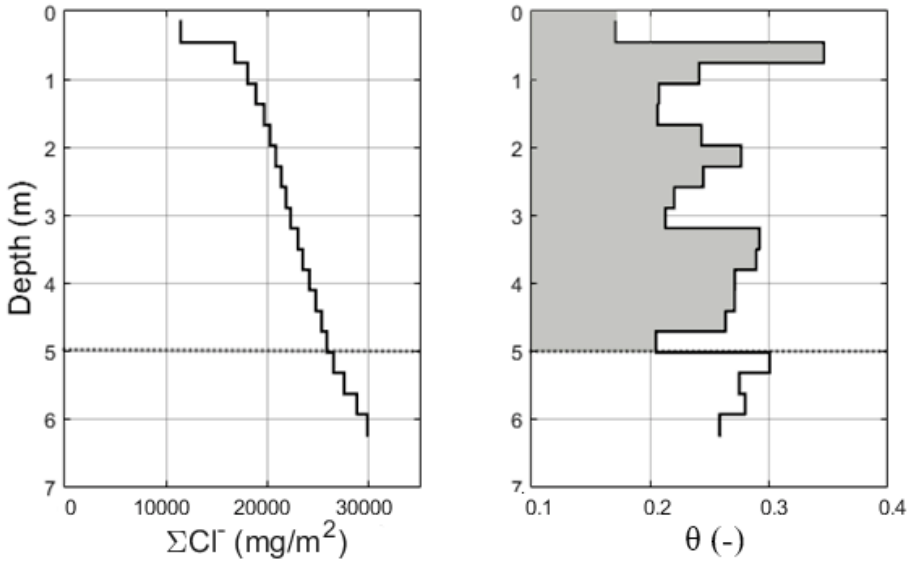

Figure 2.2: Assuming an approximate 26,000 mg/m^2 of Cl^- was applied from precipitation and irrigation over 2008-2012, the depth of deep drainage water from 2008 to 2012 would be 5 m (dashed line). Deep drainage water is calculated as depth-integrated water content over this interval. (Figure adapted from Healy, 2010).

Annual irrigation application amounts were in part determined by in-field measurements, as well as from the Tri-Basin Natural Resources District (NRD) reported flow meter data obtained from Grassini et al. (2015). Irrigation water was sampled twice in the month of July during the first growing season. Due to storm damage to the center pivot systems in the second growing season, additional irrigation water sampling was not possible.

A nearby HPRCC weather station was used to inform annual precipitation rates. Cl^- concentrations of rainwater were calculated through an inverse distance weighting (IDW) function. The data used in the IDW function was from the following North American Deposition Program (NADP) weather stations: North Platte, NE; Mead, NE; and Lake Scott State Park, KS (NADP, 2014).

In the process of crop development, both soybean and corn plants uptake a small but significant amount of Cl^-. This Cl^- is partitioned into both the stover and either the grain

or bean (Bennett, 1993). During harvest, the Cl^- in the grain or bean is removed from the field, referred to as Cl^- harvest export (CHE) (Bennett, 1993; Ward, 2010). Only a handful of deep drainage studies have considered this effect (Liao, 2012; Lin, 2013), and further study is needed to better constrain both the uptake amounts, and how much it varies.

Cumulative Cl^- amounts applied over the study period (2008-2013) were calculated by adding both applied irrigation water Cl^- mass inputs, as well as precipitation Cl^- mass inputs and then subtracting the estimated CHE mass due to harvesting the crop. Cumulative chloride at depth in each extracted soil core was determined from each sampled gravimetric water content (u (-)), Cl^- concentration, and interval the sample represented (30 cm). With the known mass of applied chloride over the previous five years, the depth of deep drainage water representing the last five years was determined. Average deep drainage was then calculated as depth-integrated water content over this interval. Volumetric water content was calculated from gravimetric water content measurements and observed bulk density determined to be 1.4 g/cm^3.

Because land use data was available for both fields from 2005-2013 (Grassini et al., 2015), this same approach was repeated but from 2005-2013. This estimation exceeds the study period (2008-2013) but tillage practice for both fields was consistent through these additional years (Deck, 2010). Although this estimation includes increased temporal uncertainty (specifically Cl^- concentration in irrigation water), a greater depth of extracted cores is able to be utilized, and the impact of the root zone in the deep drainage estimate is decreased.

In most deep drainage estimation studies, only one soil core per study area is extracted and analyzed. In this study, 3 cores were extracted in each field. If chloride mass

balance (CMB) estimations for each group of 3 cores are significantly different, it could be due to spatial variability, or due to noise introduced by the method.

In order to explore the collective impact of error in input parameters used in the CMB method, a Monte Carlo probabilistic error analysis (MC) was carried out using a program written in MATLAB. A MC analysis is advantageous when compared to a simple sensitivity analysis (e.g. high, medium, and low values of parameters) as its probabilistic nature allows a frequency distribution of an output (deep drainage) around the mean value, to be determined. Because frequency outputs are rarely perfectly normally distributed, mean and median values of outputs between a MC analysis and a simple sensitivity analysis will be different. The process of utilizing a MC analysis is explained in more detail in Appendix A.

The error sources considered, their range, and their assumed distribution are summarized in Table 2.1. From the known mean, standard deviation, and distribution, values of each variable in the CMB calculations were randomly selected. Following the variable selection, a deep drainage rate was calculated for each specific combination. This process was carried out a total of 10,000 times for each extracted core.

Table 2.1: Parameter error ranges used in the CMB Monte Carlo Analysis.

Error Source Considered	Error Range	Assumed Distribution
Flow Meter Measurement (gal)	+/- 5%	Normal
Cl^- Concentration of each Extracted Core Sample (ppm)	+/- 10%	Normal
Cl^- Concentration of Irrigation Water (ppm)	+/- 10%	Normal
u (-)	+/- .005	Normal
Bulk Density (g/cm^3)	+/- .1 g/cm^3	Normal

2.3.3 Lysimetry

In each field, a passive wick lysimeter (Decagon Drain Gauge G2®) was installed at a depth of 3 m. The installation hole was dug with the assistance of an auger Geoprobe® and backfilled to an approximate field bulk density. Data was collected every 1 hr and recorded on a Decagon EM5™ datalogger.

The passive wick lysimeter works in principal by diverting downward-flowing infiltrated water into a collection reservoir. The collected water then flows onto a hanging wick that applies a constant tension, and whose length is equivalent to the tension exerted (unit gradient). As long as the constant tension of the wick is similar to the surrounding soil, divergence between flowing infiltrated water and the top of the lysimeter is avoided. Divergence is also avoided with the use of a collection tube that is installed at the top of the device. Because the wick is suspended in the device, saturation is avoided as water drips off of the wick and onto a tipping bucket mechanism. The tipping bucket mechanism quantifies the amount of water flowing through the wick by tracking the number of times the bucket tips due to being full of water.

With the possibility of creating diverging or converging flow to the lysimeter in mind, an additional experimental method was used in the no-till field that is able to resolve deep drainage event dynamics. This method uses two extensometers installed in separate boreholes and at different depths – in this case at 3.6 and 5.5 m. The purpose of these sensors is to track the strain of the surrounding soil, which changes as applied weight (water) is increased (e.g. precipitation and irrigation) or decreased (e.g. deep drainage, runoff, evapotranspiration) (Murdoch, 2015). However, due to significant data gaps as the result of technical issues, this method was not able to provide a deep drainage estimate.

The data that was collected along with some brief interpretations is presented in Appendix B.

2.3.4 Water Retention Functions

Water retention functions for extracted soil were determined experimentally in the lab. A falling head test (evaporative) was conducted through the use of a UMS soil HYPROP® system. In order to conduct the experiment, a soil core was packed into a soil core ring where field bulk density was attempted to be held constant. The soil was then saturated, two tensiometers were inserted at different depths in the soil, and then the apparatus was placed on a precision balance. Each experiment would last approximately 1 week where the conclusion of the experiment was determined when the upper tensiometer would cavitate (approximately -900 cm). Bulk density was then measured by drying the soil in an oven for 24 hours at 100^{o}C. Van Genuchten fitting parameters were determined with the use of the UMS HYPROP® fitting function software (Pertassek et al., 2015).

2.5 Buckingham-Darcy

In both fields, pressure head sensors (Watermark™) were installed at 2.4 and 2.7 m depths. Hourly measurements were recorded on a Campbell Scientific data logger from the period of May 27th to September 17th, 2013. This provided the time series necessary to determine the pressure head gradient below the root zone.

With a known pressure head gradient below the root zone, along with water retention functions measured in the lab, seasonal deep drainage estimations were determined from hourly flux calculations based on Buckingham-Darcy law:

$$q = -K(h)\left(\frac{\partial h}{\partial z} + 1\right) \tag{5}$$

where q is equal to flux (cm/hr), *h* is pressure head (-cm), *K(h)* is unsaturated hydraulic conductivity between the upper and lower pressure head sensors (cm), and *z* is the distance between the upper and lower pressure head sensors (cm). *K(h)* was determined through the use of the relative hydraulic conductivity equation as outlined in van Genuchten, 1980:

$$K(h) = K_s \frac{\{1-(\alpha h)^{n-1}[1+(\alpha h)^n]^{-m}\}^2}{[1+(\alpha h)^n]^{m/2}}, \qquad (m = 1-\frac{1}{n}) \tag{6}$$

where K_s is saturated hydraulic conductivity (cm/day), n is a dimensionless fitting parameter in the van Genuchten equation, and α (1/cm) is a fitting parameter in the van Genuchten equation.

Pressure head time series provide a useful indication of soil water potential seasonal dynamics. However, caution must be exercised when they are used to estimate deep drainage rates. Uncertainties stem from poorly constrained water retention fitting parameters (Radcliffe and Šimůnek, 2010), as well as from the accuracy of the soil water potential sensor measurements.

In order to determine the collective effect of water retention fitting parameter errors (α, n, and K_s) along with the error of each soil water potential sensor (assumed +/-10% of reading), on deep drainage rates, a probabilistic error analysis (Monte Carlo) was performed with the aid of MATLAB. This step was taken in order to contextualize results of the method with calculated density function around mean values of reported deep drainage rates.

2.4 Results and Discussion

2.4.1 Soil Core Analysis

Results of the 190 sample soil core analysis are displayed in Figures 2.3 and 2.4. Table 2.2 describes average profile data from the analysis. Surprisingly, average gravimetric moisture contents were comparable in both fields, while Cl^- concentrations differed significantly.

The till field north, central, and south cores had average gravimetric water contents of .201, .191, and .208, respectively. At the near surface, moisture contents were low and Cl^- concentrations were correspondingly high. This is likely due to evapotranspiration concentrating pore water solute concentrations. Observed sharp changes in moisture and Cl^- concentration are likely the result of borehole cave-in or from topsoil falling down the borehole during the extraction process.

The no-till field north, central, and south cores had corresponding average gravimetric water contents of .213, .193, and .209. Cl^- concentrations were approximately 50% of those in the till field. This difference may be due to lower evapotranspiration, as well as lower concentration of Cl^- in applied irrigation water in the no-till field. Further study is needed to explain the difference in Cl^- concentrations in irrigation water for fields in such close proximity.

In both fields, below 2 m a general increase of Cl^- concentration at depth is present. Additionally in both fields, a bulge of Cl^- is observed at an approximate depth of 10 m. The cause of this increase in Cl^- concentration is unclear, but changes in land management (namely irrigation application or crop rotations) is a possible contributing factor.

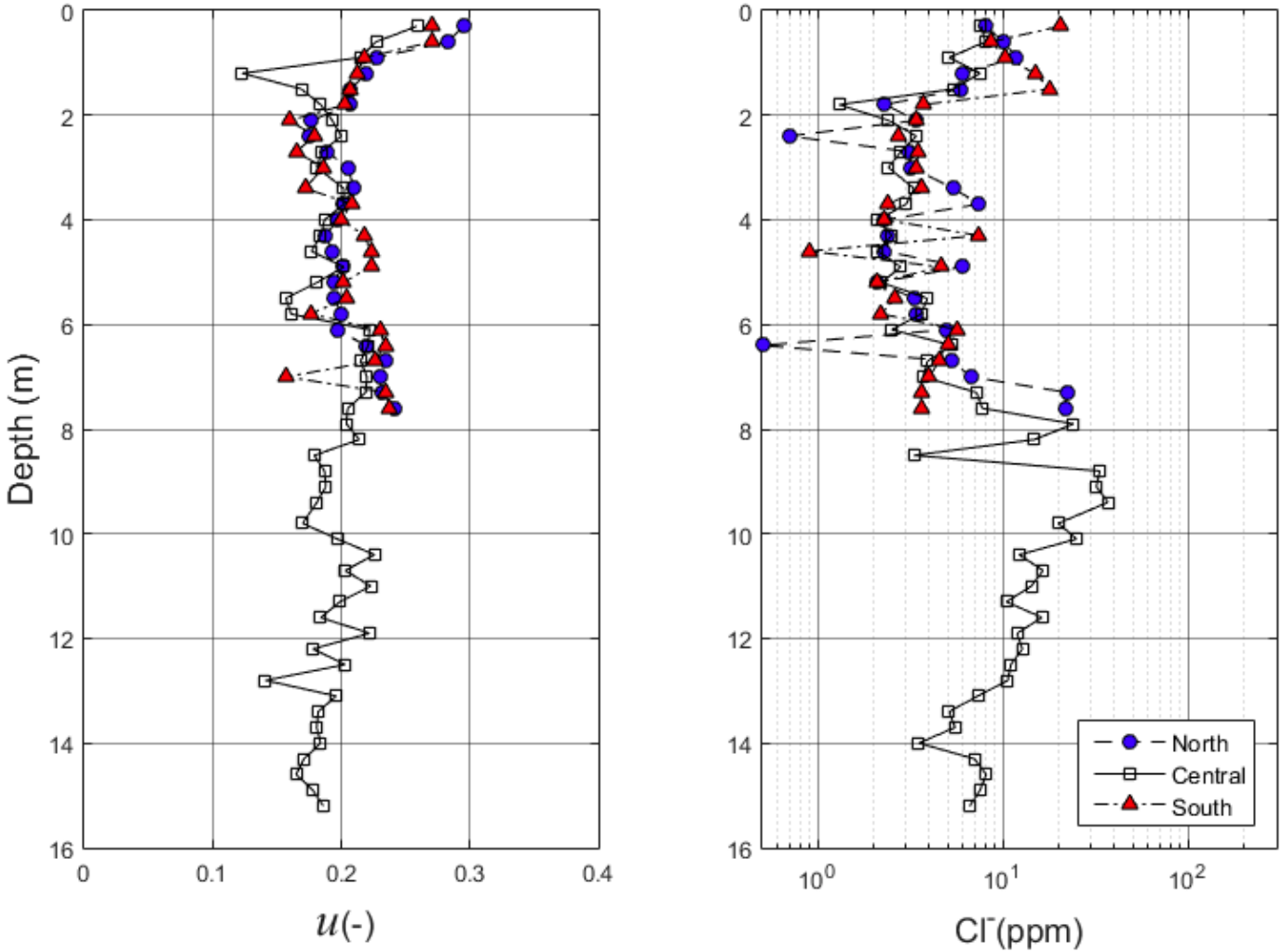

Figure 2.3: No-till field extracted core gravimetric moisture (u), and Cl^- profiles.

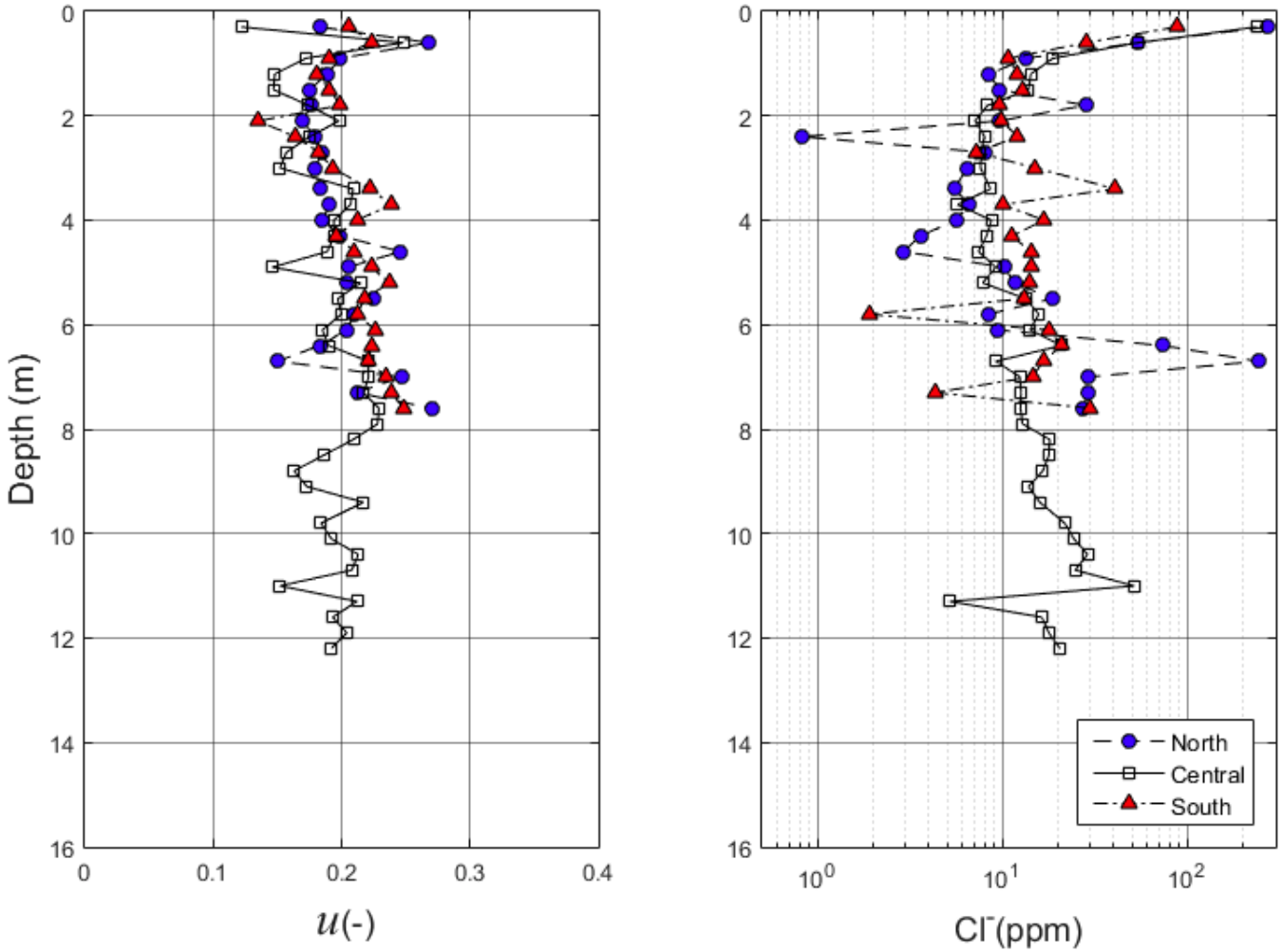

Figure 2.4: Till field extracted core gravimetric moisture (u), and Cl^- profiles.

Table 2.2: Average u(-) and Cl^- (ppm) for each extracted core.

Tillage	Core	Core Depth (m)	Average *u* (-)	Average Cl^- (ppm)
Disk	North	7.6	0.201	35.6
	Central	12.2	0.191	21.2
	South	7.6	0.208	17.2
No-till	North	7.6	0.213	6.0
	Central	15.2	0.193	9.1
	South	7.6	0.209	5.7

2.4.2 Chloride Mass Balance

In both fields, irrigation water was the predominant source of Cl^-. Cl^- concentrations of the irrigation water were 20.8 ppm in the till field, and 10.6 ppm in the no-till field. Average annual irrigation application in the till field was 231 mm and 153 mm in the no-till field for the 5 growing seasons considered in the analysis. This led to an average annual Cl^- input of 4800 mg/m^2 in the till field and 1600 mg/m^2 in the no-till. Irrigation for both fields is presented in Table 2.3. This data was from NRD flow meter data and not measured in either field. As a result, this data may be inaccurate.

Table 2.3: Annual irrigation application as reported by in-field flow meters.

Year	2005	2006	2007	2008	2009	2010	2011	2012	2013
Till (mm)	285	246	No Data	226	213	109	170	437	467
No-till (mm)	218	160	187	117	127	89	150	284	193

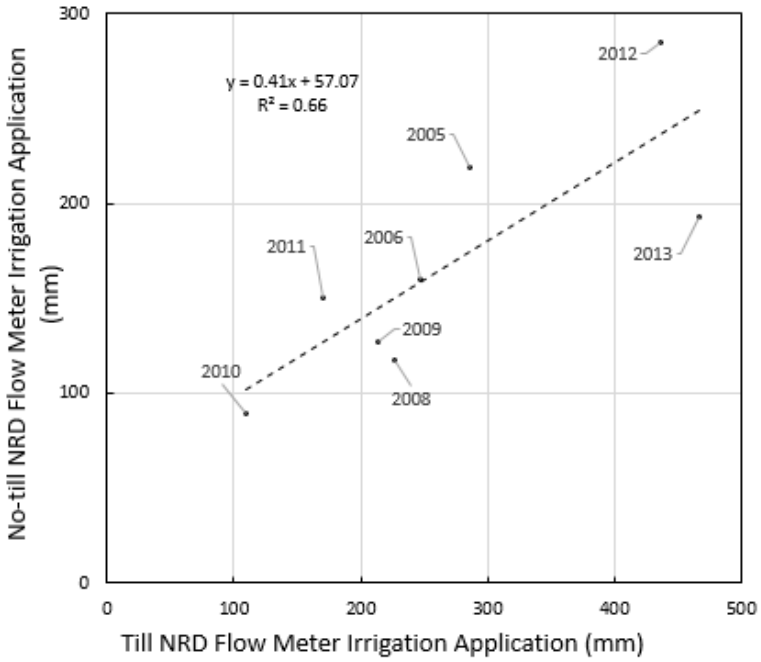

Figure 2.5: Annual irrigation application for both the till and no-till fields as measured by the in-field NRD flow meters.

Over the study period, average annual rainfall was 570 mm/yr and average Cl^- concentration was .067 ppm. Average annual atmospheric Cl^- inputs to both fields were 38 mg/m^2. When compared to irrigation, Cl^- input from precipitation is not a significant term in the CMB equation as it contributes less than 3% of total Cl^- input. Additionally, this is why the study period was rounded to 5 years instead of 5.4 (soil core extraction occurred on May 28th, 2013). Because CMB tracks time through accumulated Cl^- input and soil core extraction occurred prior to the 2013 irrigation season, only a small amount of Cl^- had been applied to the field at the time of extraction.

With the known amount of applied Cl^- during the study period, the depth of deep drainage water occurring over the study period was found to be 2.4 m in the till field and 6.5 m in the no-till field (central cores only). The depth of deep drainage water was multiplied by depth-integrated volumetric water content over the depth that represented the

last 5 years of drainage, and drainage rates of 110 mm/yr in the till field, and 350 mm/yr in the no-till field were determined (central cores only). However, these drainage estimations do not consider relatively important sources of error in the CMB equation.

Table 2.4: Precipitation, irrigation and Cl^- concentrations used in the CMB equation.

Year	Precipitation (mm)	IDW Precipitation Cl^- concentration (ppm)	Till Irrigation (mm)	Till Irrigation Cl Concentration (ppm)	No-till Irrigation (mm)	No-till Irrigation Cl Concentration (ppm)
2008	671.4	0.066	226	20.88	117	10.61
2009	494.9	0.065	213	20.88	127	10.61
2010	738.1	0.057	109	20.88	89	10.61
2011	593.9	0.076	170	20.88	150	10.61
2012	348.1	0.071	437	20.88	284	10.61
2013	147.6*	0.085	0*	0	0*	0

*Amount up to May 29th – the day of soil core extraction.

In order to consider important sources of error in the CMB equation, a Monte Carlo probabilistic analysis was preformed to determine the collective impact of considered error sources on deep drainage rates. For each core this analysis was carried out on, computational time took approximately five minutes. The number of calculations selected (10,000) was observed to be sufficient as probability density functions did not change appreciably when calculations were increased.

Figure 2.6 summarizes the results of the Monte Carlo analysis. Mean values for the till field north, central, and south cores were, 40, 110, and 210 mm/yr, respectively. Mean values for the no-till north, central, and south cores were, 100, 350 and 240 mm/yr, respectively. Deep drainage density plots with a log-normal distribution tended to have higher Cl^- concentrations at the top of the profile than other cores. Normally distributed density plots were the result of fairly linear cumulative Cl^- concentrations at depth in the core considered. Overall, the analysis indicated that error constraints had a secondary

impact on deep drainage rates when compared to the effect of spatial heterogeneity or perhaps noise introduced by the methods used for analysis (e.g. Geoprobe® extraction).

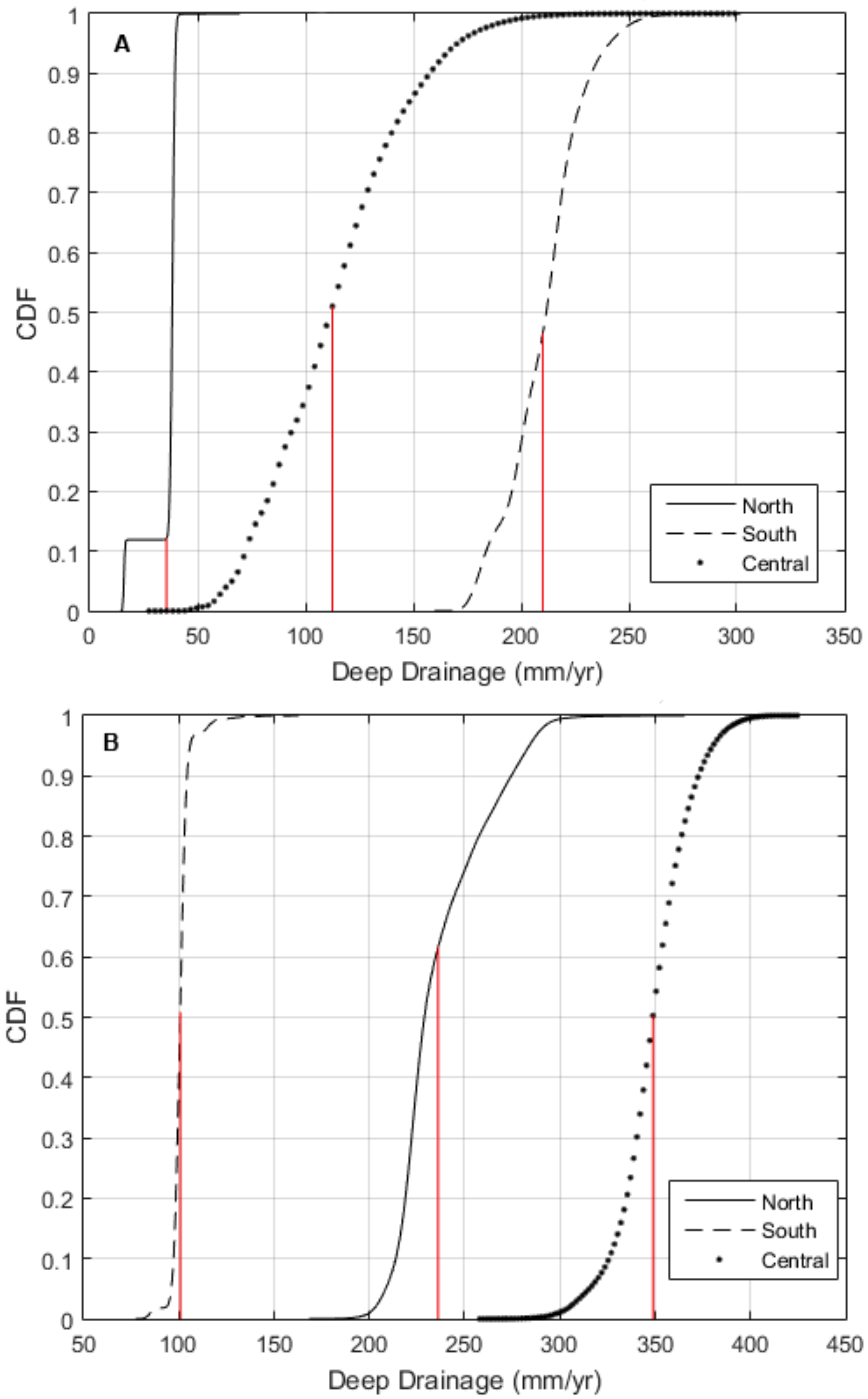

Figure 2.6 Cumulative distribution function (CDF) for CMB MC deep drainage calculations representing average deep drainage over 5 years for the A) till and B) no-till field. Red lines indicate mean values of deep drainage.

A geophysical survey conducted on the no-till field indicated a general lack of soil texture spatial heterogeneity (Appendix B). Additionally, loess soils tend to be fairly homogenous due to consistent depositional processes. This would suggest that differences observed between cores within the same field may be more attributable to the methods used in the analysis and not to spatial heterogeneity. If this is the case, averaging the measurements at depth between the three cores in each field may mitigate the error induced by the methods imposed. Figure 2.7 is the density plot of the same Monte Carlo analysis but with averaged soil core measurements between all 3 soil cores in each field. Table 2.5 presents the results of this analysis along with the percentage of deep drainage to irrigation and precipitation. The percentage of deep drainage to irrigation plus precipitation for both fields is comparable to Klocke et al. (1999), who reported a 6 year average of 26-34% for a corn/soybean rotation in North Platte, NE, under a silt loam soil.

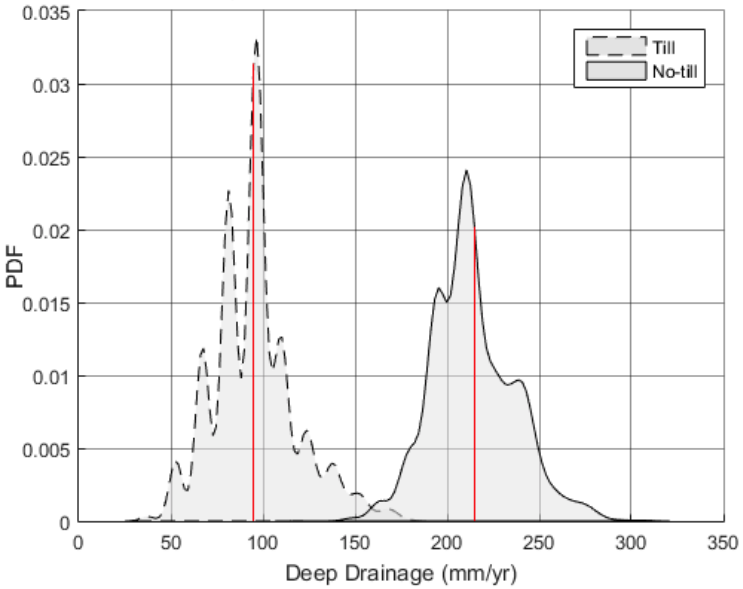

Figure 2.7: Probability density function (PDF) of average deep drainage rates calculated from the CMB equation with averaged soil moisture, and averaged Cl^- concentration profiles for each field. Red lines indicate mean deep drainage rates.

This analysis was repeated over the extended period of 2005-2013. Average deep drainage for the till and no-till fields was 200 and 260 mm/yr respectively. The average depth of deep drainage water representing this interval for the till and no-till field was, 5.9 and 7.1 m respectively. Results of this analysis can be seen in Figure 2.8 and in Table 2.5.

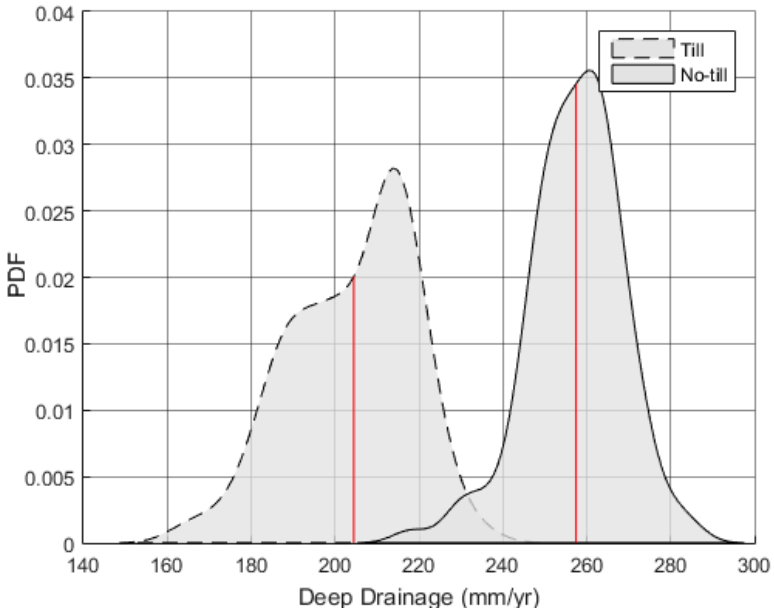

Figure 2.8: Probability density function (PDF) of average deep drainage rates calculated from the CMB equation over the period of 2005-2013 with averaged soil moisture, and averaged Cl^- concentration profiles for each field. Red lines indicate mean deep drainage rates.

Table 2.5: 5 and 8 year average CMB deep drainage estimates for averaged cores and corresponding values of precipitation and irrigation.

Tillage	Years Considered	Average Precipitation + Irrigation (mm/yr)	Average Deep Drainage (mm/yr)	Average Deep Drainage % of Average Precipitation + Irrigation
Till	2008-2013	810	100	12.3
No-till	2008-2013	730	210	28.8
Till	2005-2013	850	200	23.5
No-till	2005-2013	780	260	33.3

2.4.3 Lysimetry

For the 2013 growing season, 248 mm of deep drainage was measured in the till field while 42 mm of deep drainage was measured in the no-till field. This was over the time period of May 27th to September 17th. Irrigation amounts determined by the in-field and out-of-field rain gauge for the season are presented in Table 2.3 and 2.7 respectively. The in-field and out-of-field rain gauge derived irrigation amounts differ from the reported flow meter data, and it is uncertain as to why this is. Difference in the application amounts between the two fields are the result of independent decision making by the land owners. Notably, some irrigation events were quite small as recorded by the rain gauge. It is unclear if this was the actual irrigation amount or if irrigation was actually higher but debris may have somehow interfered with the in-field rain gauge.

In the till field, most deep drainage events captured by the lysimeter occurred after mid-July. This coincides with irrigation application increasing in early July. Drainage rates were observed to be as high as 12.4 mm/day.

In the no-till field, total drainage amount was much lower than in the till field. Only three main drainage events were picked up by the lysimeter and two of the three events are likely the result of irrigation giving the timing of the response. The maximum daily drainage event was comparable to the till field at 12.1 mm/day.

In both fields, by mid-season, the lysimeters demonstrated a good response to precipitation and irrigation. In the early part of the growing season, drainage events may have been missed due to divergence as a result of installation. Figure 2.11 is a qualitative attempt to link precipitation and irrigation with drainage events in the till field. Due to a lack of events in the no-till field, this analysis was not carried out. Looking at Figure 2.11,

it can be seen that the time in between irrigation and precipitation events is generally mirrored in the time between each drainage event. Additionally, the total number of drainage events matches the total number of irrigation and precipitation events over the growing season. It is uncertain if preferential flow led to this strong response between wetting events at the surface, and drainage. This is a known possibility when disturbing soil and installing soil water sensors in any field installation. With this in mind, at installation extracted soil was packed back to approximate field bulk density and soil was replaced in the same order it was extracted in. Appendix C also explores this drainage dynamic through the use of an extensometer.

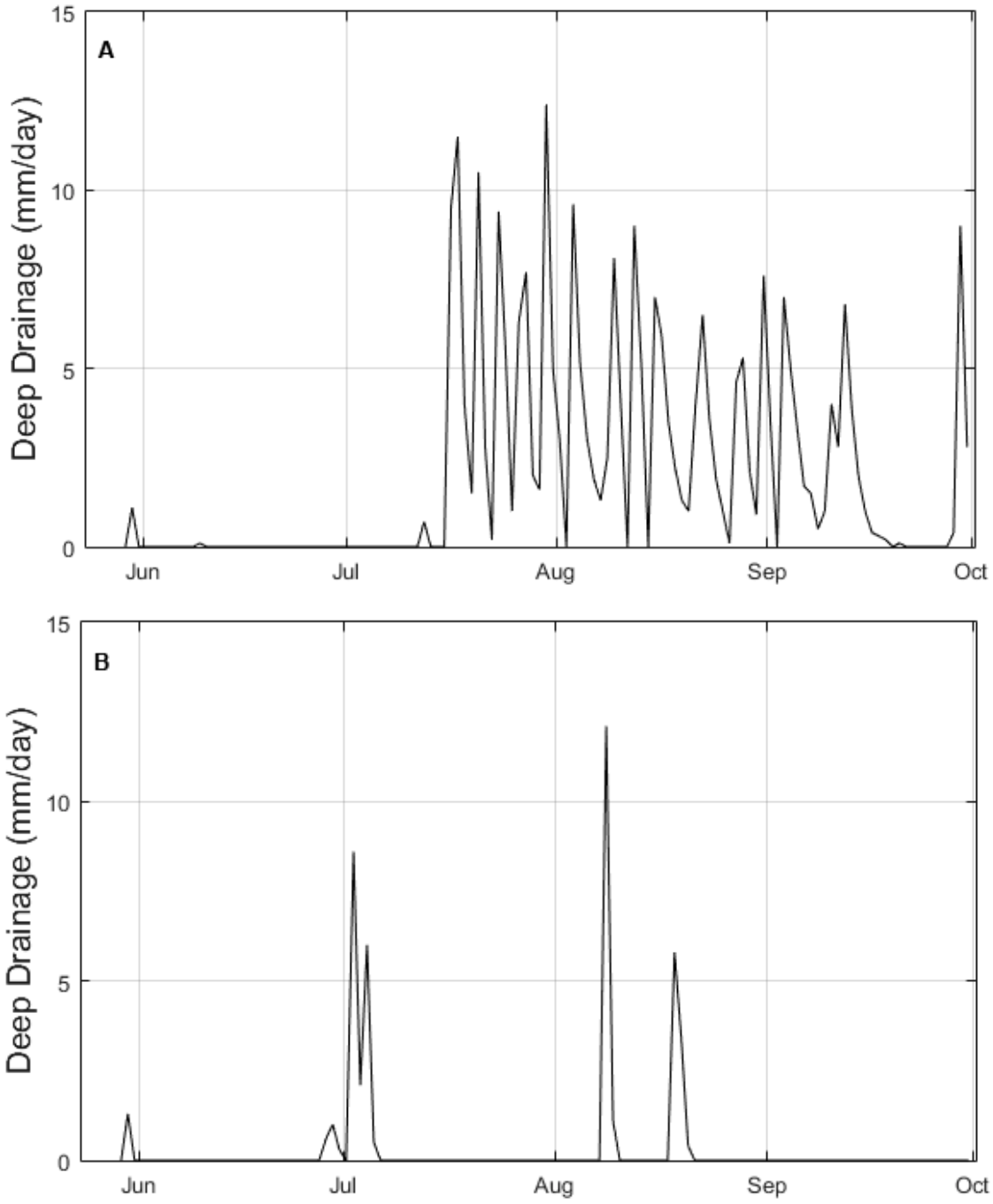

Figure 2.9: Deep drainage in the A) till field and B) no-till field over the 2013 growing season as measured by the lysimeters. Note that the in the till field (A), time between each drainage peak is about 3-4 days. This time lag is similar to the time the center pivot needs to move around the entire field.

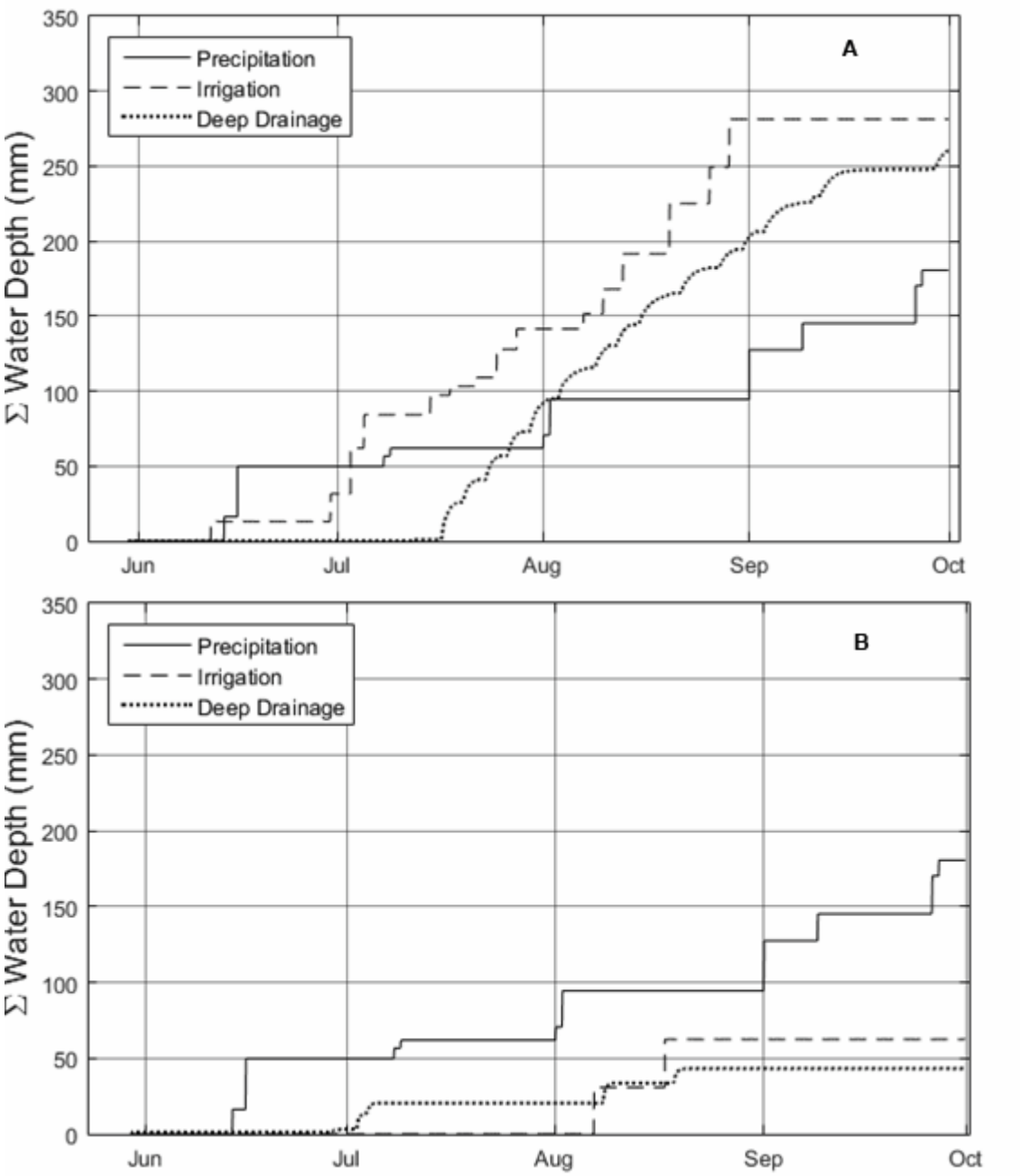

Figure 2.10: Cumulative precipitation, irrigation, and drainage over the 2013 growing season for the A) till and B) no-till fields.

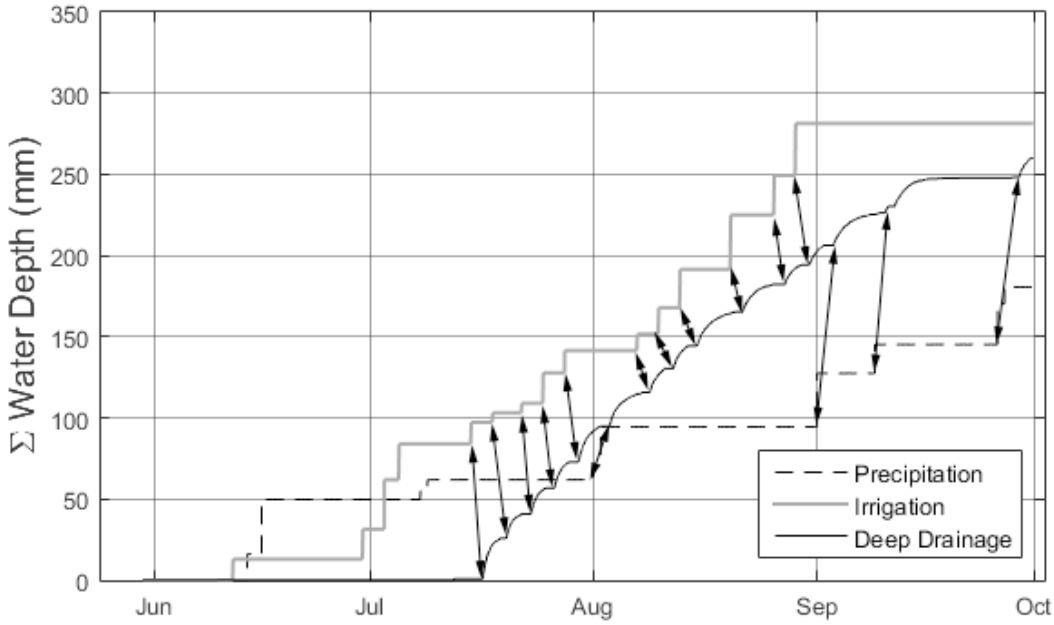

Figure 2.11: Qualitative analysis of both irrigation and precipitation events and their corresponding drainage events.

Table 2.6: Irrigation application (mm) in each field for the 2013 growing season as reported by the in-field rain gauge.

Till Field Irrigation		**No-till Field Irrigation**	
Date	**Amount (mm)**	**Date**	**Amount (mm)**
6/12/2013	13.0	8/8/2013	30.7
6/30/2013	18.5	8/18/2013	31.7
7/3/2013	30.5		
7/5/2013	22.1		
7/15/2013	13.2		
7/18/2013	5.8		
7/22/2013	5.8		
7/25/2013	18.8		
7/28/2013	13.7		
8/7/2013	10.2		
8/10/2013	16.3		
8/13/2013	23.6		
8/20/2013	33.5		
8/26/2013	24.4		
8/29/2013	32.0		
Total	281.4		62.4

2.4.4 Water Retention Functions

Water retention data for soil samples extracted from both the till and no-till fields are presented in Table 2.7 and Figure 2.12. Saturated hydraulic conductivity values are within reason of a silt-loam soil when compared to samples from the soil database ROSETTA (Schaap et al., 2001). Porosity values are fairly agreeable from sample to sample, with a range of 0.5-0.58 being in the range for a silt-loam. Residual water content values were assumed as that parameter was too far outside the range of measurement of the soil HYPROP (0 cm to approximately -1000 cm of pressure head).

Table 2.7 Van Genuchten fitting parameters for soil samples measured in lab.

Sample Name	Depth of Sample (m)	Tillage of Field Extracted From	θ_r (-)	θ_s (-)	α (1/cm)	n (-)	K_s (cm/day)
WS02	0.3	Till	0.067	0.577	0.0198	1.205	21.5
SC1	surface	No-till	0.067	0.542	0.0621	1.089	77.2
FS08	2.4	No-till	0.067	0.506	0.0035	1.849	7.2
WS08	2.4	Till	0.067	0.563	0.0080	1.200	89.9

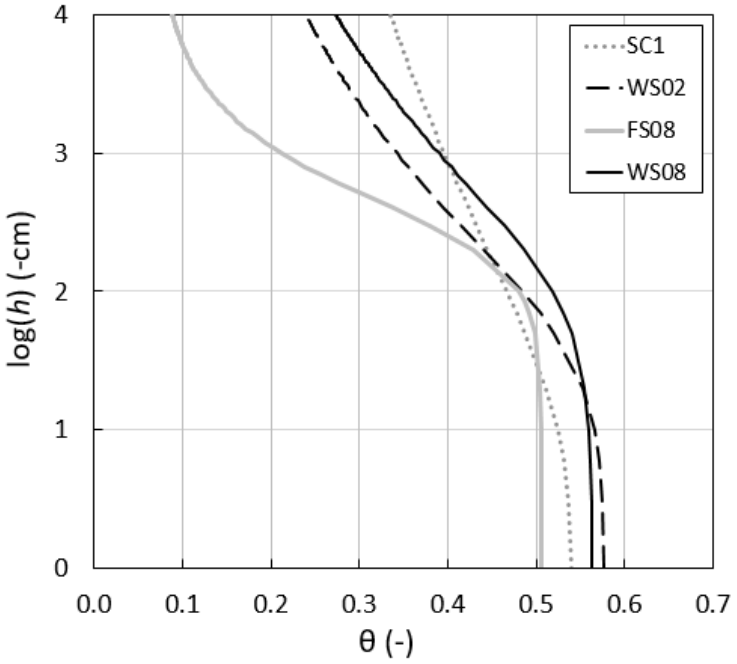

Figure 2.12: Water retention curves for soil samples measured in lab.

2.4.5 Buckingham-Darcy

The results of the pressure head sensors installed at 2.4 m and 2.7 m for both fields can be seen in Figure 2.13. Over the course of the growing season, both fields were near field capacity (approximately -300 cm) indicating a relatively moist subsurface.

In the till field, the pressure head sensors show that the field is generally becoming more wet throughout the growing season. This trend appears to line up with the increase in irrigation application around the same time. Additionally the Buckingham-Darcy drainage estimation has a very similar seasonal trend as the installed lysimeter (Figure 2.14). A minor drainage event early in the season (May 31st) was indicated by the pressure head sensors but not by the lysimeter. This may indicate some divergence occurring above the lysimeter due to installation, but by mid-season, both the pressure head sensors and lysimeter were indicating similar deep drainage rates.

In the no-till field, the two pressure head sensors diverge around mid-July and show an upward flux or negative deep drainage occurring over the last half of the growing season. It is unclear if this is an actual trend, a sensor failing, or due to some problem at installation. The lack of change in reading from early August to late September suggests the sensor may have malfunctioned after installation. Additionally, given the relatively close proximity of the two sensors (30 cm apart), it would be likely that the two would show similar magnitudes of change in pressure head over time.

Results of the Monte Carlo analysis can be seen in Figure 2.15. Deep drainage rates around the calculated mean for the till and no-till field were significant. Negative deep drainage rates in the no-till field are likely the result of a malfunctioning sensor.

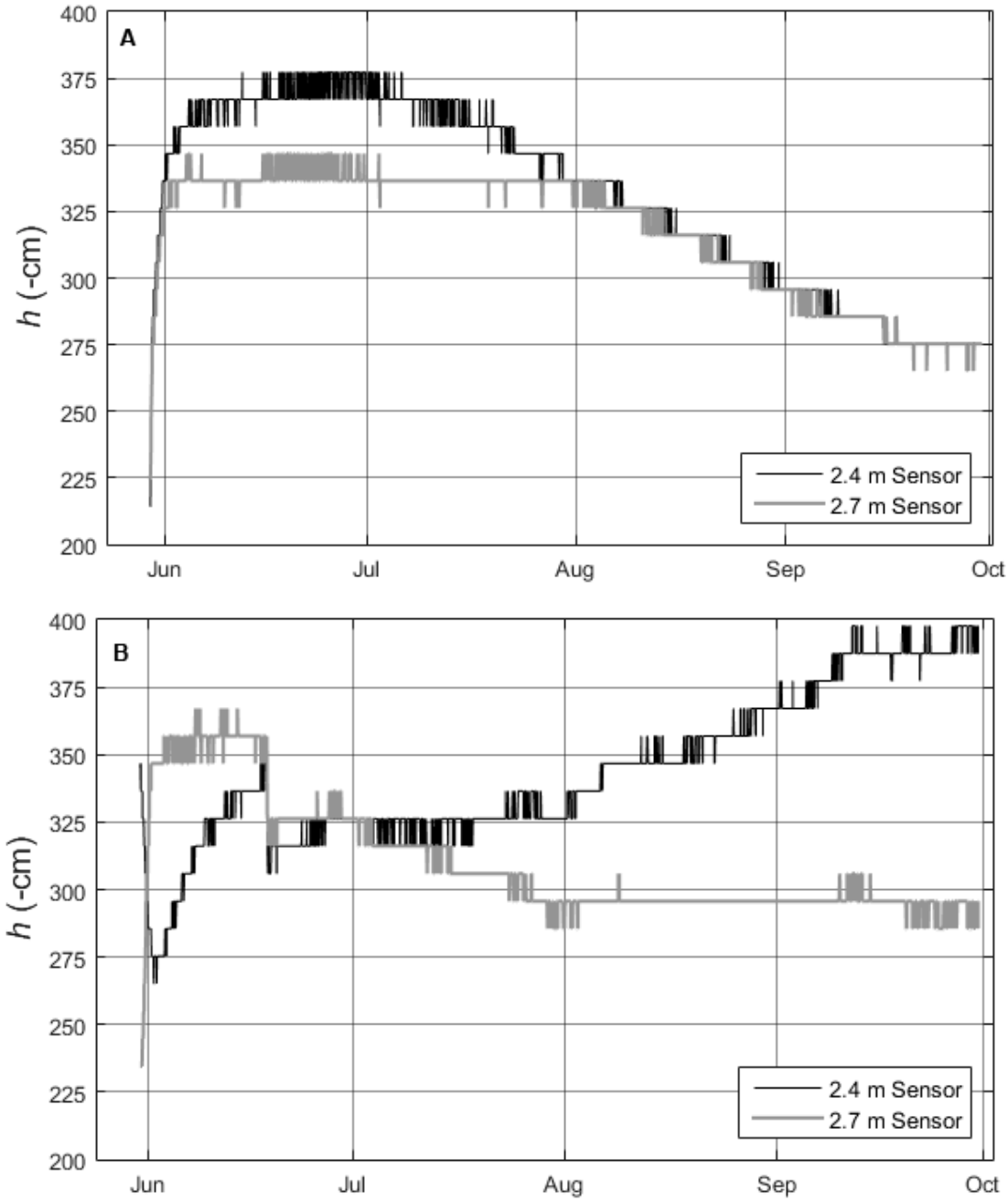

Figure 2.13 A) till and B) no-till field pressure head (*h*) time series for the 2013 growing season.

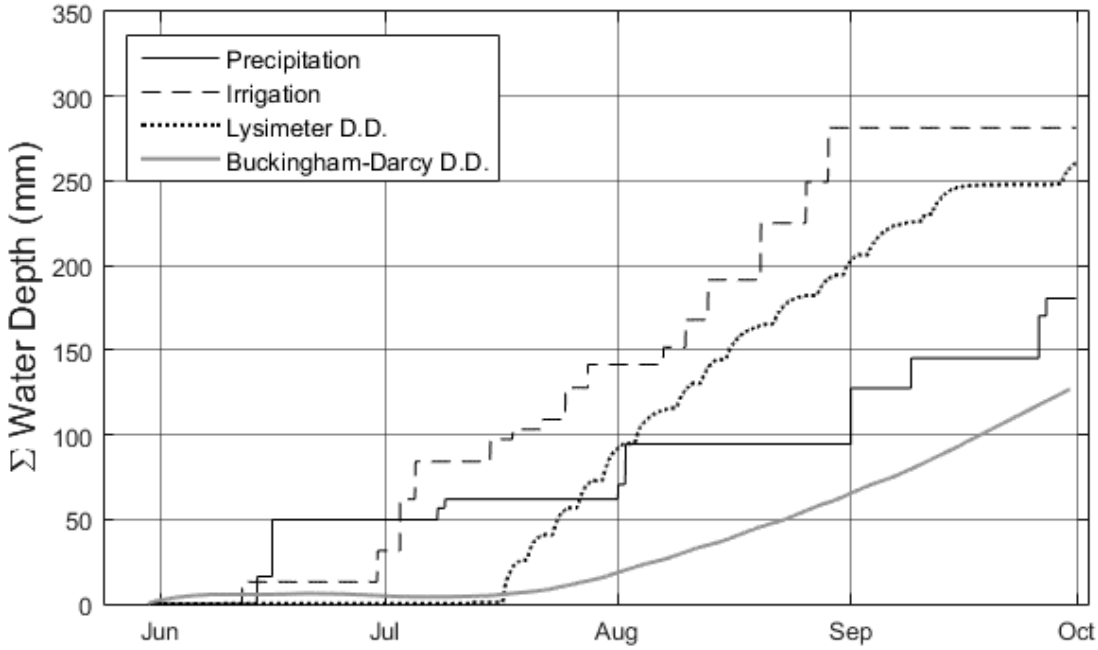

Figure 2.14: Cumulative precipitation, irrigation, and deep drainage (DD) measured by a lysimeter and from Buckingham-Darcy.

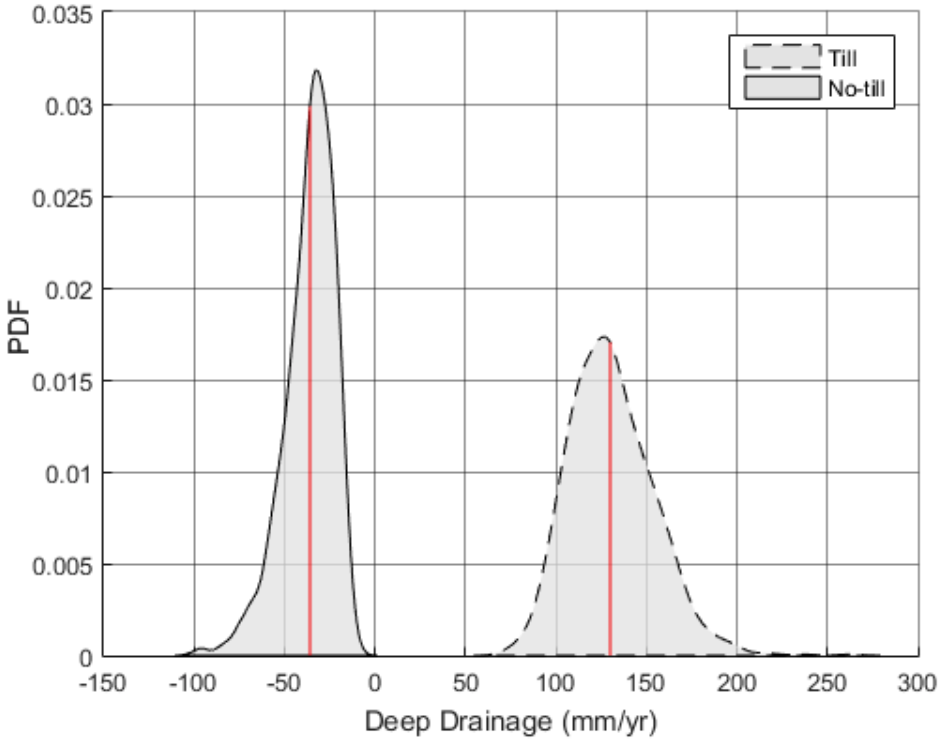

Figure 2.15: Probability density function (PDF) of deep drainage as calculated by the MC analysis for the Buckingham-Darcy method. The upward (negative) drainage in the no-till field may be due to a sensor malfunction. Red lines indicate mean deep drainage rates.

2.4.6 Comparison of Previous Deep Drainage Estimates

Additional deep drainage estimations were completed from the same core data determined in this analysis (Bosch, 2015). The additional methods were nitrate peak displacement and darcy-law unit gradient (DLUG). The NPDM method is an additional chemical tracer method and DLUG is an additional physical-indirect method.

The NPDM tracks peaks of nitrate in deep drainage water where the peaks represent annual inputs of nitrogen to the field for fertilization. Deep drainage was estimated by multiplying the distance in between nitrate peaks by volumetric water content, following the methods of Bobier et al. (1993) and Katupitiya et al (1997). This method determined deep drainage rates of 286 and 260 mm/yr for the no-till and till fields respectively.

The DLUG method determines a range of depth within the core that has consistent volumetric water content. This area is then assumed to be under unit gradient – defined where drainage is the result of the force of gravity (Healy, 2010). Unsaturated hydraulic conductivity is determined from the known volumetric water content. Deep drainage is then equivalent to this unsaturated hydraulic conductivity. Results of this method were 210 and 155 mm/yr for the no-till and till fields respectively.

The magnitudes of the results of these methods are similar to the CMB method previously described in this chapter, and they both indicate greater deep drainage in no-till than in till. These methods represent an important additional source of deep drainage estimation. Both methods were not impacted by disturbing of soil at installation. Additionally, both of these methods would not have been impact by the significantly different irrigation application observed in 2013 as they were determined from extracted cores removed prior to irrigation in 2013.

2.5 Summary and Conclusions

Three methods were employed to estimate deep drainage between two experimental fields located in south central Nebraska. In-field physically based deep drainage estimations indicated that a greater amount of deep drainage occurred in the till field (250 mm) than in the no-till field (50 mm) over the 2013 growing season. The tracer-based deep drainage estimate indicated more deep drainage in the no-till field (210 mm) than in the till field (100 mm) over the 5 years considered in the analysis. The source of this discrepancy is believed to be in part due to differences in irrigation application between the two fields over a single full growing season (2013), which was not representative of the long-term land management practices of both fields. Additionally, due to consistent differences in irrigation application over the 5 years considered in the chemical tracer analysis, it is difficult to determine the impact of tillage on deep drainage by directly comparing deep drainage rates. However, these estimates represent an important component to determining the impact of tillage on the water balance as a whole.

Uncertainty analysis of both the physical indirect method (Buckingham-Darcy) and the chemical tracer method (CMB) indicate significant ranges of deep drainage rates around the reported means. These analyses add transparency to methods that have significant parameter uncertainty. The lack of overlap of deep drainage estimations between the two tillage fields within the same method suggests that the methods selected are sufficient for determining the impact of tillage on deep drainage.

Both methods of physical deep drainage monitoring indicated deep drainage was occurring late in the growing season and possibly into the fall. Surprisingly no technique indicated deep drainage occurring in the beginning of the growing season when

precipitation is frequent and potential evapotranspiration tends to be lower. Monitoring for longer periods of time during the year would be an improvement on the techniques in order ensure significant deep drainage events were not missed outside of the growing season.

Monitoring for only one entire growing season was conducted. Because the timing and magnitudes of precipitation, irrigation, and potential evapotranspiration are different every year, this leads to estimations that have a high degree of temporal uncertainty. Additionally, the installation of soil-water sensors disturbed the surrounding soil. Although the soil was repacked back to restore field bulk density, a longer period of time would have allowed the soil to settle. For this reason, an additional year was planned to monitor deep drainage. Unfortunately a hail storm prevented a second year from being monitored. Even with a second year of measurements, measured deep drainage rates may have still been prone to uncertainties.

Chapter 3: Assessing the Mechanisms Leading to Differences in Deep Drainage Rates Under Irrigated Till and No-till Agriculture with Unsaturated Zone Numerical Modeling

3.1 Introduction

The sustainability of both groundwater quantity and quality under irrigated agriculture is heavily impacted by the timing and rates of deep drainage (Klocke et al., 1999; Spalding et al., 2001; Scanlon et al., 2008; and Exner et al., 2014). The timing and rates of deep drainage are predominantly the net result of the influence of two primary drivers in the water balance – precipitation and potential evapotranspiration – on soil-water dynamics. Unfortunately, those two primary drivers often vary in both timing and magnitude from year-to-year, making short term deep drainage monitoring deterministic. In the case of irrigated agriculture, the balance between precipitation and evapotranspiration is able to be attenuated through irrigation application. However, irrigation application often varies on a producer-to-producer level even when all other factors are similar (Grassini et al., 2015). To better understand timing and rates of deep drainage, long-term monitoring on the scale of 10 years is often preferred (Scanlon et al., 2008). Decadal time scale field monitoring of deep drainage can be cost-prohibitive and as a result, numerical models are frequently turned to as a method for long-term estimation. Given the field-specific data collected and discussed in Chapter 2, an excellent opportunity to use vadose zone modeling to explore differences in deep drainage rates due to tillage practice exists.

Hydrus 1D is utilized to explore the net of effects of differences on deep drainage rates between the two tillage practices. Hydrus 1D (H1D) is a free and publicly available

one-dimensional numerical model that simulates water flow through unsaturated and saturated media (Šimůnek et al., 2013). Differences between the two fields considered in the model include: potential evapotranspiration, water retention functions, and due to the differences in irrigation application of the producers managing the two experimental fields discussed in Chapter 2, two different irrigation regimes applied to both fields. The results of this modeling exercise are not intended to be used as an additional deep drainage estimation to supplement work done in Chapter 2, but rather to indicate important sources of differences in seasonal and long-term soil water dynamics.

Previous work has shown that vadose zone models have a high sensitivity to poorly-constrained input parameters (Wang et al., 2009). With that in mind, careful attention is paid to bracketing the sensitivity of H1D to input parameters, through the use of a probabilistic uncertainty analysis. The aim of this uncertainty analysis is to contextualize the previous model simulation results with important error sources, as well as the distribution of deep drainage rates around the reported mean. Additionally, an error analysis comparison is made between two different methods to obtain water retention parameters. The first is a pedotransfer function, a method that is popular in vadose zone modeling, and the second is a laboratory measured water retention function. Pedotransfer functions trade ease of use for greater parameter uncertainty, while laboratory measurements tend to have less uncertainty at the expense of time and effort.

3.2 Methods of Numerical Modeling

3.2.1 Vadose Zone Model

Soil water dynamics for both fields were simulated using the numerical model, HYDRUS 1D (H1D). Full discussion of the H1D code is outside the scope of this chapter, however salient aspects of the code will be highlighted and discussed. H1D simulates water flow by approximating the 1D Richards equation:

$$\frac{\partial \theta}{\partial t} = \left(\frac{\partial}{\partial z} \right) \left[K(\theta) \left(\frac{\partial h}{\partial z} + 1 \right) \right] - S \tag{8}$$

where θ is volumetric water content (-), t is time (day), z is distance between pressure head measurements (cm), $K(h)$ is unsaturated hydraulic conductivity, h is pressure head (-cm), and S is a sink term describing evapotranspiration (1/day).

3.2.2 Weather Data

Twelve years of weather data were obtained from a HPRCC weather station located in south central Nebraska (HPRCC, 2014). This location was chosen due to its geographic proximity to both fields (approximately 5 km) monitored in the previous chapter. Weather data considered in the model includes: potential evapotranspiration, precipitation, and irrigation.

3.2.3 Estimation of Potential Evapotranspiration

Potential evapotranspiration (ET_p) was estimated for both fields by in part following the single crop coefficient method outlined in FAO 56, 1998:

$$ET_c = ET_{NE} K_c \tag{9}$$

where, ET_c is crop specific potential evapotranspiration, ET_{NE} is reference crop ET_p calculated from micro-meteorological variables, and K_c is a dimensionless empirical

constant that encompasses crop development as well as the average effect of soil on evaporation rates. Daily ET_{NE} data was determined from HPRCC weather station data. Previous work has indicated different evaporative potential for crop residue covered soil, as opposed to bare soil (Klocke et al., 2009; Odhiambo and Irmak, 2012). In order to consider this effect, different sets of K_c values for the till and no-till fields were used. K_c values published by HPRCC were appropriate to use for the till field as they are representative of conventional farming practices in the state. K_c values for no-till that were specific to the region were unavailable. Because of this, they were calculated from Ameriflux data (Ameriflux, 2013) collected at a research site near Mead, NE. This process is discussed in more detail in Appendix D with a calibration exercise also presented. In both cases, K_c values were calculated as a function of growing degree day accumulation (GDD) after planting instead of the fixed day growing stages as outlined by FAO 56, 1998. A single day calculation of growing degrees (GDD_{daily}) is defined as:

$$GDD_{\text{daily}} = \frac{Temp_{\max} + Temp_{\min}}{2} - Temp_{\text{base}} \tag{10}$$

where, $Temp_{max}$ is equal to the daily maximum temperature (^oC) (or 30^oC whichever is smaller), $Temp_{min}$ is equal to the daily minimum temperature (^oC), and $Temp_{base}$ is equal to 10^oC. The GDD method is preferred as it more accurately represents a proxy for crop development, as opposed to a fixed number of days after planting. This is because GDD accumulation is not consistent from year-to-year, and growth stages of corn are believed to follow GDD accumulation (Yang et al., 2013).

The H1D model requires ET_c be partitioned into its separate components – evaporation and transpiration. This is accomplished through the use of Beer's law:

$$T_p = ET_c\left(1-e^{-k*LAI}\right) \quad (11)$$

$$E_p = ET_c - T_p \quad (12)$$

where Tp is potential transpiration, Ep is potential evaporation, ET_c is crop specific potential evapotranspiration, k is the light extinction coefficient (set to .55) and LAI is leaf area index of the crop. One LAI multi-year seasonal dynamic was simulated through the use of Hybrid-Maize, to represent both fields. Hybrid-Maize is a UNL produced crop modeling software that simulates the development of maize under well-watered and water stressed conditions (Yang et al., 2013). Hybrid Maize was also utilized to estimate date of silking for each year simulated.

Although the experimental fields in discussed in Chapter 2 were under a corn/soybean rotation, only corn is simulated in work done in this Chapter. This was decided as the goal of this modeling work is not to produce an additional deep drainage estimate for work done it Chapter 2 but rather determine sources of differences in deep drainage rates. Additionally, adding the increased level of complexity for simulating two crops is unjustified when growing season ET_c of soybean is within 10-15% of corn in the simulated region (Sharma and Irmak, 2012).

3.2.4 Irrigation Regimes

Two irrigation regimes were considered in the model. The first irrigation regime is an irrigation scheme believed to be representative of crop management practices in south central Nebraska (Dean Eisenhauer personal communication, 2014). Starting on June 25th and ending on August 25th, 19 mm of water was applied every 3 days, but a 1 day delay to irrigation occurred for every 6.4 mm of rain that fell during each rain event

but not to exceed a delay of 7 days. The second irrigation regime was triggered by an algorithm that considers pressure head on a daily timescale at three depths (30 cm, 60 cm, and 90 cm) in the top 90 cm of the simulated profile. The trigger point for irrigation follows the recommendations outlined in UNL's extension paper on the Watermark irrigation system (Irmak et al., 2014). The specifics of how this algorithm was integrated into H1D will be discussed in detail later this chapter.

The motivation behind two different irrigation regimes stems from the differences in irrigation application of the producers managing the two experimental fields discussed in Chapter 2. Both irrigation regimes were applied to both fields, leading to two sets of simulations for a total of four simulations. This is an attempt to consider the effects of tillage, specifically potential evapotranspiration and water retention properties, on deep drainage, outside the effect of producer irrigation bias. Also, it will help explore the impact of irrigation on deep drainage rates when the two fields are irrigated identically. Additionally, both the magnitude and timing of irrigation application impact the dynamics of soil-water movement. The precipitation delayed irrigation regime, henceforth referred to as IR_{PD}, considers only the input of precipitation but not that of actual evapotranspiration (ET_a), deep drainage, and ultimately water stress due to over or under-irrigation. This is contrasted with the pressure head triggered irrigation regime, henceforth referred to as IR_h, which is driven by pressure head. Pressure head can vary drastically in both time and depth and is the result of water application, ET_a, deep drainage, and soil-water properties. The IR_h is designed to irrigate only when needed, defined by soil-water availability.

3.2.5 Soil Profile Information

A 6 m soil profile split into two layers represented the vadose zone in the simulations. The upper layer (UL) was 65 cm deep and the no-till and till profiles had soil water parameters assigned from samples SC1 and WS02 respectively, while WS08 and FS08 represented the lower layers (LL) for the no-till and till soil profiles (refer to Table 2.7). The depth of the upper layer was determined from field observations. Free drainage was set as the boundary condition for the bottom of the profile, and deep drainage was measured as flux occurring at 2 m. The initial condition for the soil profile was set at -200 cm of pressure head and to avoid any impact of this initial condition, the first year of the 12 year simulation was omitted from results.

3.2.6 Coupling of HYDRUS 1D and MATLAB

In order to carry out certain seasonal dynamics unavailable in the H1D model, such as root growth with a specified distribution and triggered irrigation, MATLAB was used to execute the H1D code on a single day basis. At the end of a one day simulation, model outputs (pressure head at depth, flux rates, actual evapotranspiration, etc.) were read and stored within a matrix in MATLAB. H1D files were then created via MATLAB by outputting the soil profile at the end of the previous day as the new initial condition for the next day, making sure to match the format of H1D input files. The H1D executable was then called and the profile information at the end of the next one day simulation was read again. This process was repeated 4383 times which then comprised the ensemble 12 year simulation for each tillage and irrigation regime.

In the case where a simulated day occurred during the growing season, root depth and distribution inputs were calculated on a daily basis based off of a pre-determined

GDD accumulation after planting for each growing season. This process was carried out following the equations outlined in the Hybrid Maize user manual:

$$Root\ Depth\ =\ \frac{GDD}{GDD_{\text{Silking}}} MRD \tag{13}$$

$$Root\ Distribution = \exp(-VDC\ Depth_{\text{layer}} / Root\ Depth) \tag{14}$$

where, $GDD_{silking}$ is equal to growing degree days at silking, *MRD* is a biophysical parameter representing the maximum depth the root zone will reach (cm), exp is the natural exponential function, *VDC* is a vertical distribution coefficient, and $Depth_{layer}$ is the current depth in the root zone (cm).

The single day reading and writing of input and output files allowed for a customized algorithmic irrigation scheduling that would not normally be possible in H1D. The algorithm worked by checking if the simulated day occurred between June 25th and August 25th, then the pressure heads at 30, 60, and 90 cm depths were tracked. When the pressure head at those 3 depths (top 2 depths prior to silking date as determined by Hybrid Maize) was -1000 cm or less, a 25.4 mm irrigation event was added as precipitation in the model for the following day. The tracked depths and pressure head trigger point of this algorithm was consistent with recommendations outlined by Irmak et al. (2014).

3.2.7 Error Sources in Vadose Zone Modeling

Few studies have quantified important error sources within vadose zone models. Previous work has indicated that vadose zone models have a high sensitivity to input parameters (Wang et al., 2009). With this in mind, 2 irrigation regimes and 3 input parameters were selected for an investigation that was conducted in order to determine their collective effect on deep drainage rates. Irrigation regimes considered are the same

as discussed in section 3.2.4. Two of the three input parameters selected for this investigation were soil-water parameters defined by the van Genuchten (VG) equation: α, and n. The third parameter considered is a biophysical parameter representing the maximum depth the simulated vegetation's roots will grow to, referred to as the maximum rooting depth (*MRD*). Mean values and range of this parameter are defined in Table 3.1 (Suat Irmak, personal communication, 2014).

There are two primary approaches to determine soil-water parameters for a given soil: empirically and experimentally. The empirical approach is popular in vadose zone modeling as it only requires basic textural information (% sand, silt, clay, and bulk density values), which is entered into a pedotransfer function (PTF) that correlates texture to VG parameters. An experimental method to determine soil-water parameters in the lab (LM) was discussed in Chapter 2.4.4. With these soil water parameters, a water retention function (WRF) can be determined. Both methods lead to parameter error, with empirical methods typically having higher parameter error. Error distributions for both α, and n, were determined for both methods from outputs from each method's respective program (ROSETTA and HYPROP) and for both layers of soil in order to keep consistent with the profile as described in section 3.2.5. These values are presented in Table 3.1. Because sufficient data was collected in Chapter 2 to utilize both methods, the two methods will be compared to each other in the uncertainty analysis.

In this analysis, only the till field was simulated. This was decided because the purpose of the analysis is to contextualize the simulated mean deep drainage rates for the no-till and till fields, with important sources of error. Because the two fields were

parameterized in a similar manner, important error sources should have similar roles in both fields.

3.2.8 Monte Carlo Probabilistic Error Analysis

Due to numerous nonlinearities in soil-water dynamics, determining the effect of model parameter uncertainty on deep drainage rates is not a straightforward process. A useful method to probabilistically determine the collective effect of dependent variable uncertainty, on independent variables, is a Monte Carlo analysis. A Monte Carlo analysis was carried out by first defining mean values, standard deviations, and distributions of each parameter considered (*α, n, and MRD*, see Table 3.1). Next, with the use of MATLAB, a combination of the considered model parameters was determined by probabilistically drawing values from the known distributions. This combination was then run through the H1D model following the methods outlined in Section 3.2.6. This process was repeated 1000 times for each WRF method and irrigation regime (4000 total simulations) in order to ensure a stable mean, and frequency distribution was achieved.

Because the Monte Carlo analysis was computationally intense, the simulations were coded to be run in parallel within MATLAB on a University of Nebraska supercomputer, Tusker. This is an effort that is believed to be a first, and allows a large number of H1D simulations to be run in a short period of time. Parallel computing allowed 32 simulations to be ran simultaneously, with a decrease of simulation time proportional to the number of cores accessed on the computing platform reducing computation time from 10 days to 8 hours.

Table 3.1: Framework of the MC uncertainty analysis with mean values and standard deviations for each input parameter.

Irrigation Regime	Water Retention Function Measurement Method	Parameter	Mean Value (cm)	Standard Deviation (cm)	Distribution
Pressure Head Triggered (IR_h)	Laboratory Measured	α Upper Layer	0.0198	0.206	Normal
		α Lower Layer	0.008	0.174	Normal
		n Upper Layer	1.21	0.168	Normal
		n Lower Layer	1.20	0.211	Normal
		MRD	150	8.33	Normal
	Pedotransfer Correlation	α Upper Layer	0.0052	1.215	Log-normal
		α Lower Layer	0.0063	0.704	Log-normal
		n Upper Layer	1.66	1.419	Log-normal
		n Lower Layer	1.60	1.419	Log-normal
		MRD	150	8.33	Normal
Precipitation Delayed (IR_{PD})	Laboratory Measured	α Upper Layer	0.0198	0.206	Normal
		α Lower Layer	0.008	0.174	Normal
		n Upper Layer	1.21	0.168	Normal
		n Lower Layer	1.2	0.211	Normal
		MRD	150	8.33	Normal
	Pedotransfer Correlation	α Upper Layer	0.0052	1.215	Log-normal
		α Lower Layer	0.0063	0.704	Log-normal
		n Upper Layer	1.66	1.419	Log-normal
		n Lower Layer	1.6	1.419	Log-normal
		MRD	150	8.33	Normal

3.3 Results and Discussion

3.3.1 Timing and Magnitudes of Deep Drainage: Till vs No-till

Results of the H1D simulations can be seen in Figures 3.1-3.4 and are summarized in Table 3.2. Figure 3.5 highlights the deep drainage time series by overlaying all annual cumulative deep drainage time series. For both tillage practices and irrigation regimes, the primary amount of deep drainage is occurring in the springtime (April-July). Average deep drainage rates for the till and no-till fields in the case of IR_h are 120 and 210 mm/yr respectively, and in the case of IR_{PD} are 140 and 410 mm/yr respectively.

Differences in deep drainage rates between the fields primarily occur in the fall as the no-till field tends to have more frequent and larger deep drainage events when compared to the till field. The cause of this difference is believed to be primarily the result of irrigation scheduling. In both simulated fields, irrigation is stopped on August 25th. This cessation of irrigation is consistent with irrigated corn practices, with the purpose of drying out the grain and field prior to harvest (Yonts et al., 2008). During this period of time, the soil-water in both the till and no-till fields is becoming depleted due to the lack of irrigation. Because ET_c is higher in the till field than in the no-till field, the soil is relatively drier in the till field by the end of the growing season. This makes the profile relatively less conductive than the no-till field and rain events in the fall have less potential to become deep drainage. This also suggests that irrigation in the no-till field may be able to be stopped sooner than in the till field, however in both cases irrigation was stopped in a simplistic way (with a set day of year).

3.3.2 ET_a Difference: Till vs No-till

Actual evapotranspiration (*(*ET_a) time series can be seen in Figures 3.1-3.4 for all simulations. The ET_a results of the simulations are not intended to be used as a comparable field measurement for work done in Chapter 2. Instead, their purpose is to serve as a reasonable seasonal dynamic.

The long term average annual ET_a for the till field under IR_h triggered irrigation was 698 mm/yr and the long term average growing season ET_a was 632 mm/yr. The long term average annual ET_a for the till field under IR_{PD} irrigation was 706 mm/yr with a long term average growing season ET_a of 639 mm/yr. These numbers compare well to findings of other regional studies such as Szilagyi and Jozsa (2013), who report approximately 700mm/yr for the southeastern area of Phelps County, and Sharma and Irmak (2012), who report 630 mm over the growing season for corn in Phelps County.

The long term average annual ET_a for the no-till field under IR_h was 536 mm/yr and the long term average growing season ET_a was 437 mm/yr. The long term average annual ET_a for the no-till field under IR_{PD} irrigation was 432 mm/yr and the long term average growing season ET_a was 367 mm/yr. The relatively low ET_a rate under the IR_{PD} appears to be the result of water stress due to water logging. This may not be physically realistic but for this scenario, average irrigation application was significantly higher than what was observed in the field: 170 mm as opposed to the simulated 293 mm.

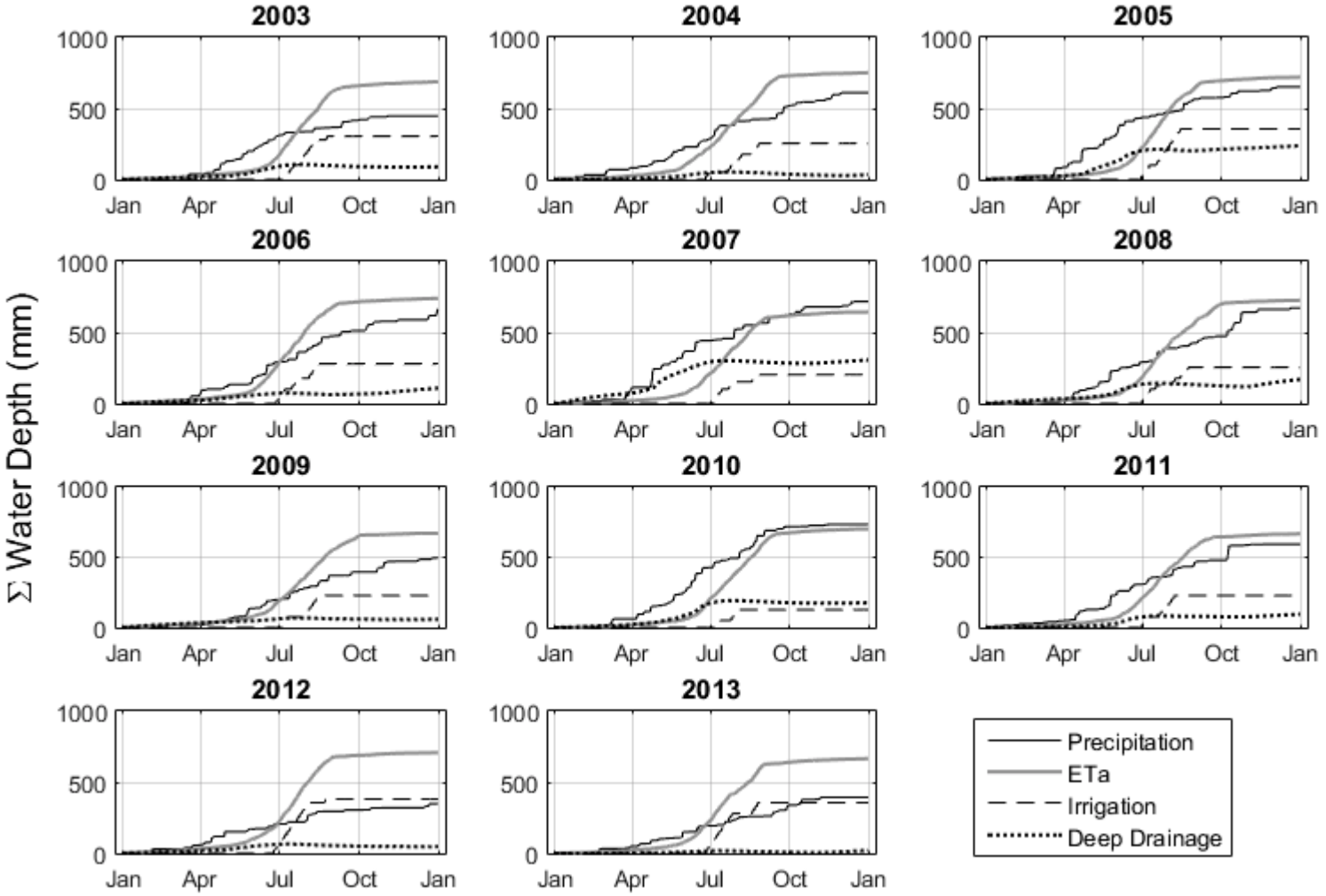

Figure 3.1: 11-year simulation results split into annual cumulative time series for the major water balance components (precipitation, ET_a, irrigation, and deep drainage) in the till field under the pressure head triggered irrigation regime (IR_h).

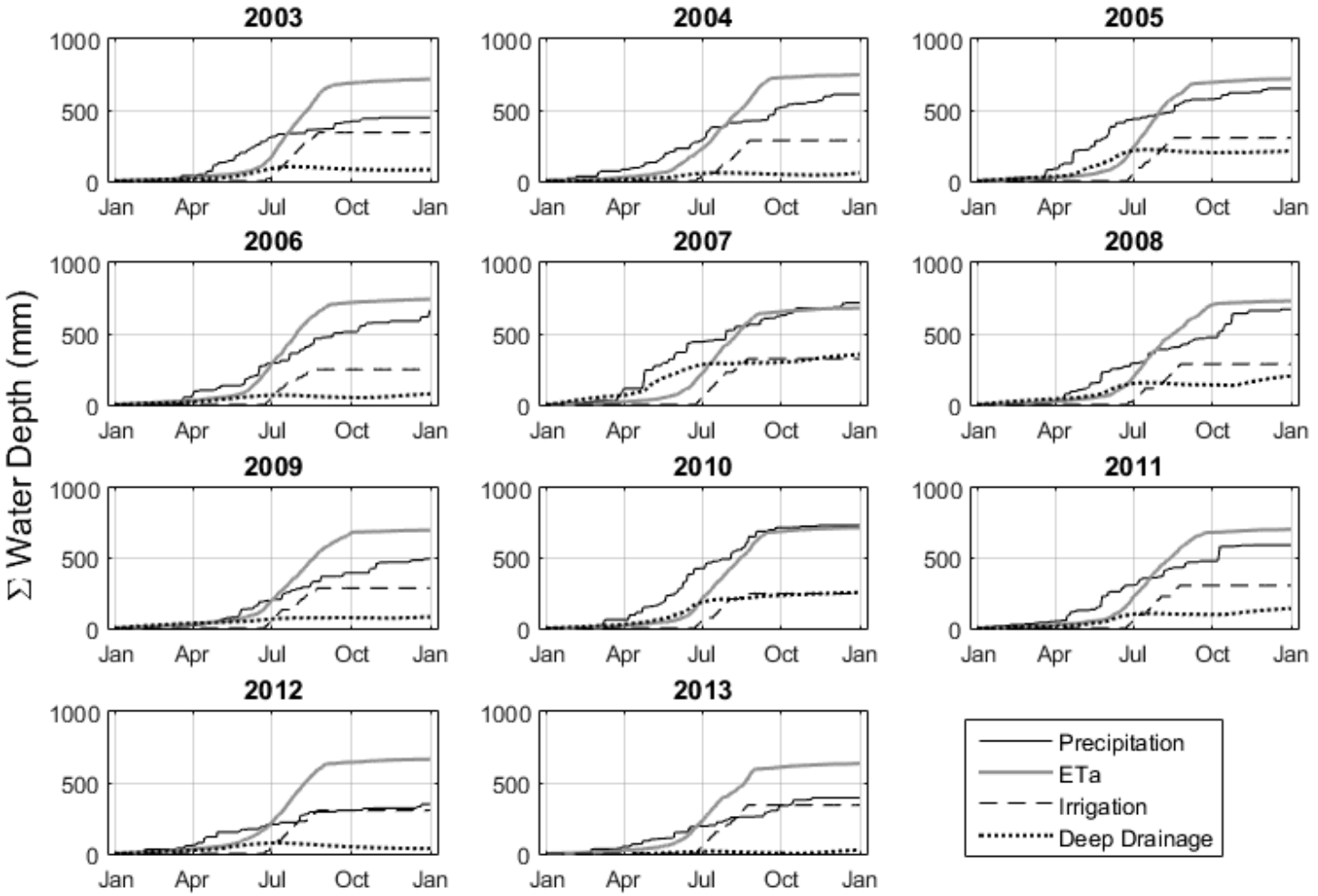

Figure 3.2: 11-year simulation results split into annual cumulative time series for the major water balance components (precipitation, ET_a, irrigation, and deep drainage) in the till field under the precipitation delayed irrigation regime (IR_{PD}).

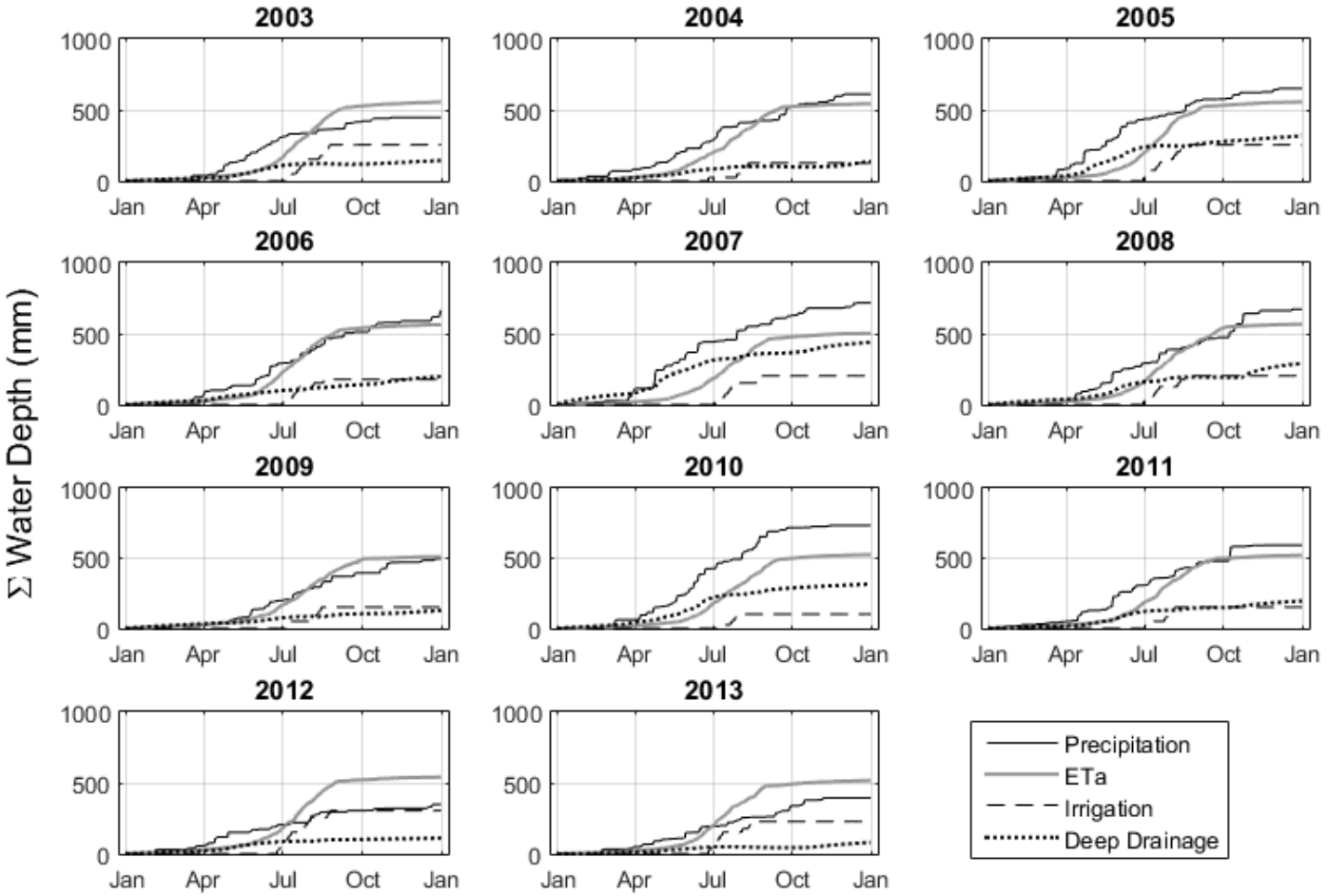

Figure 3.3: 11-year simulation results split into annual cumulative time series for the major water balance components (precipitation, ET_a, irrigation, and deep drainage) in the no-till field under the pressure head triggered irrigation regime (IR_h).

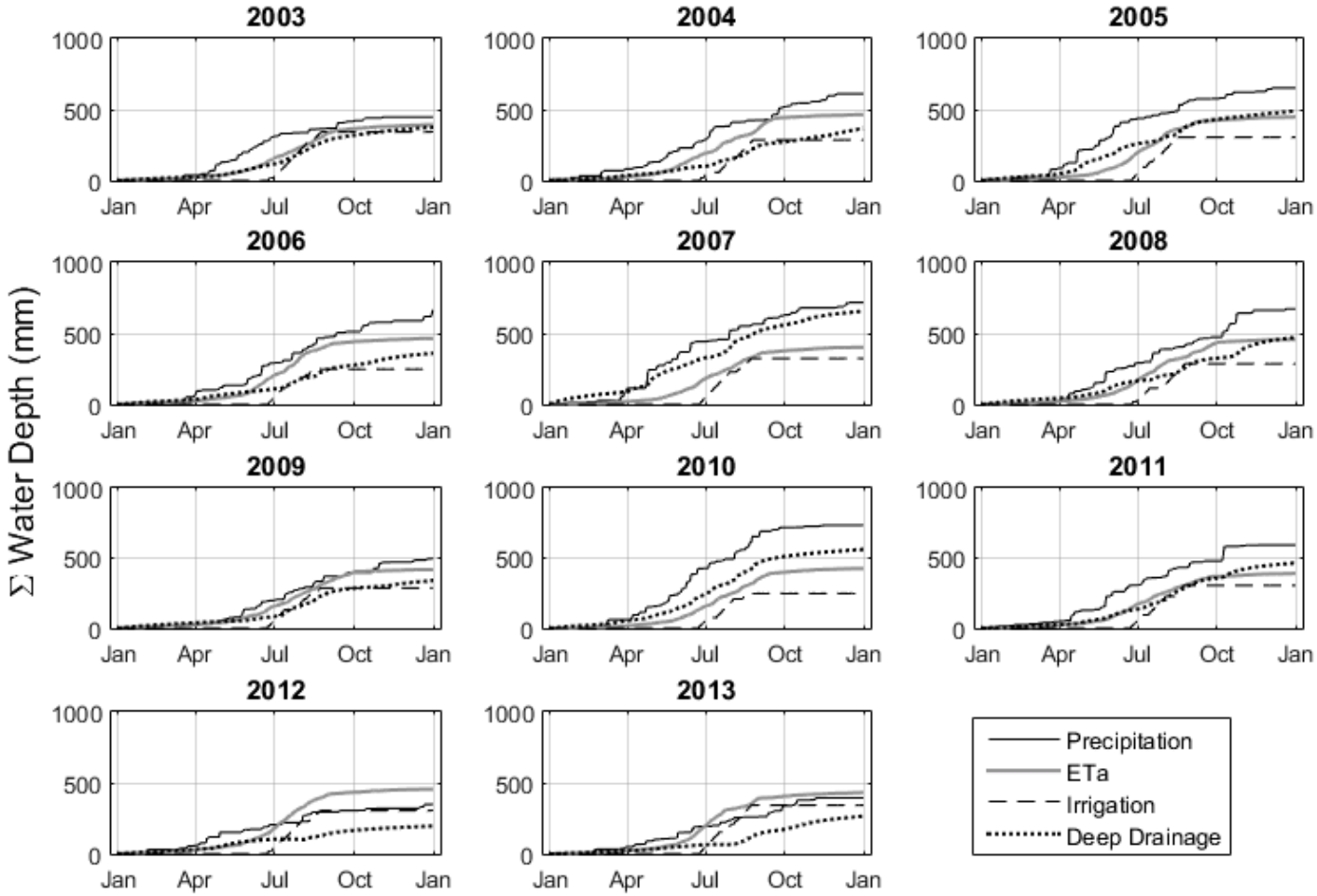

Figure 3.4: 11-year simulation results split into annual cumulative time series for the major water balance components (precipitation, ET_a, irrigation, and deep drainage) in the no-till field under the precipitation delayed irrigation regime (IR_{PD}).

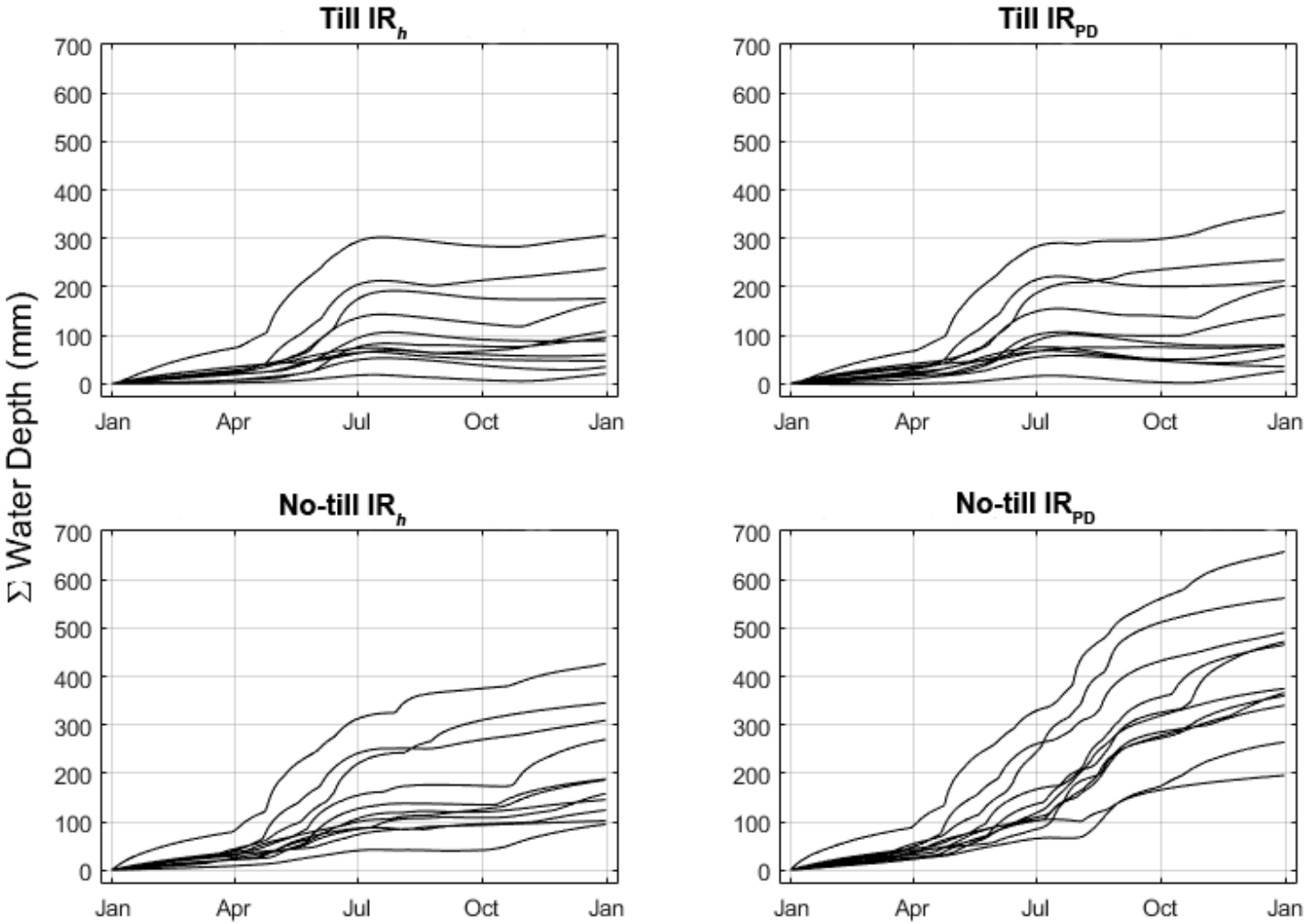

Figure 3.5: Annual cumulative deep drainage time series overlain for all years for the till and no-till fields under both irrigation regimes: pressure head triggered (IR_h) and precipitation delayed irrigation (IR_{PD}).

Table 3.2 Summary of water balance components from the H1D simulations.

2003-2013 Water Balance Summary				
Tillage	**Irrigation Regime**	**Water Balance Component (mm)**	**Mean (mm)**	**Standard Deviation (mm)**
-	-	Precipitation	576	134
-	-	Reference ETp (ET_{NE})	1685	154
Till	Pressure Head Triggered (IR_h)	ETa	698	34
		Deep Drainage	122	91
		Irrigation	270	76
	Precipitation Delayed (IR_{PD})	ETa	706	34
		Deep Drainage	138	105
		Irrigation	298	32
No-till	Pressure Head Triggered (IR_h)	ETa	537	23
		Deep Drainage	214	112
		Irrigation	196	61
	Precipitation Delayed (IR_{PD})	ETa	432	28
		Deep Drainage	413	132
		Irrigation	298	32

3.3.3 Irrigation Application

Known annual irrigation application for both of the experimental fields represent an import source of long term primary data. Comparing observed to simulated irrigation application aids in determining whether the inputs in the water balance simulated in H1D fall within a reasonable range. If simulated irrigation application is unreasonably high or low, deep drainage events may vary significantly in both timing and magnitude.

Annual irrigation application for both fields and irrigation regimes can be seen in Figures 3.6-3.7. For comparison, simulated irrigation application is plotted against the in-field flow meter measurements for each year of data. Good performance was observed for irrigation application predicted under the IR_h for both fields. Adequate performance was observed under the IR_{PD} within the till field. Although yearly application for the IR_{PD} tended to be over predicted in wet years and under predicted in dry years, average irrigation application for the observed and simulated irrigation was similar. Poor performance occurred under the IR_{PD} in the no-till field. This may be due to either decreased ET_p in the no-till field – thus requiring less irrigation – or due to the producers own irrigation tendencies.

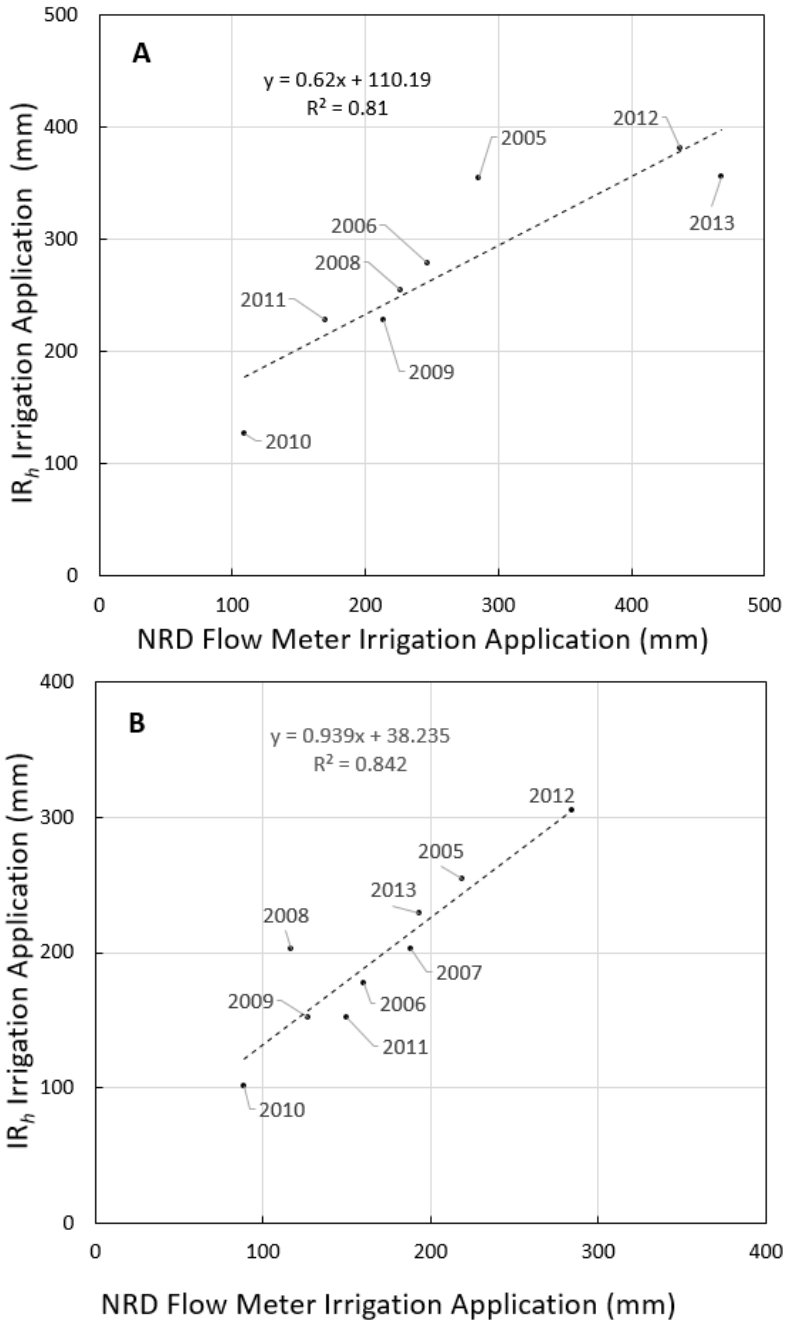

Figure 3.6 Comparison of irrigation application for the A) till and B) no-till fields as measured by the in-field NRD flow meter and estimated by the pressure head triggered irrigation regime (IR_h).

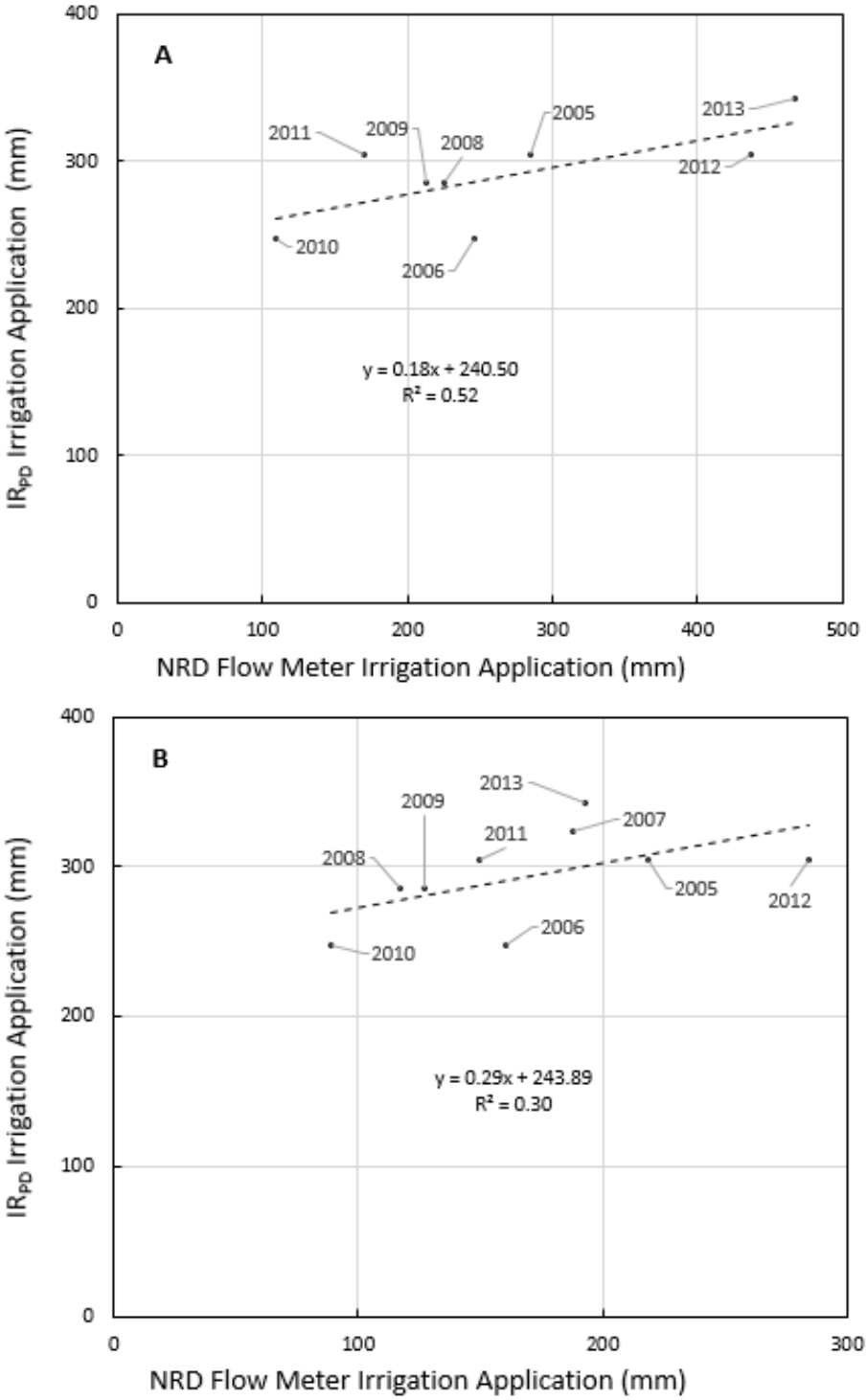

Figure 3.7 Comparison of irrigation application for the A) till and B) no-till fields as measured by the in-field NRD flow meter and estimated by the precipitation delayed irrigation regime (IR_{PD}).

3.3.4 Uncertainty Analysis

The following results and discussion sections are reported based on their category within the uncertainty analysis.

3.3.4.1 Impact of Irrigation Regime

Irrigation application regimes had a significant impact on mean deep drainage rates as can be seen in Figure 3.8. In the IR_h, 11-year average deep drainage rates were lower than IR_{PD}. This is likely the result of irrigation application being triggered as a function of soil pressure head, thereby limiting overwatering, and not by the relationship between precipitation frequency and assumed soil moisture.

3.3.4.2 LM vs. PTF Water Retention Function

Results from the uncertainty analysis show that the use of a PTF WRF leads to a higher range of deep drainage rates when compared to the LM WRF. This is likely the result of higher parameter error as can be seen in Table 3.1.

In both uncertainty analyses, the simulations ran with a WRF determined by the PTF had lower deep drainage rates. An initial thought may be that the conductivities of the two profiles may be significantly different. A common way to compare the conductivity of a profile is to compare K_s values of each material. In this case, the LM WRF has higher K_s values for both the upper and lower materials. However, even during irrigation application neither profiles reach full saturation at depth. With this in mind it is better to compare the range of K(h) and this is plotted on Figure 3.9. From this figure it can be seen that for the upper materials, other than in very wet conditions (>-100 cm pressure head), K(h) is not appreciably different. For the lower profile, K(h) is higher in

the wet range but below -300 cm of pressure head (approximate field capacity), K(*h*) becomes similar.

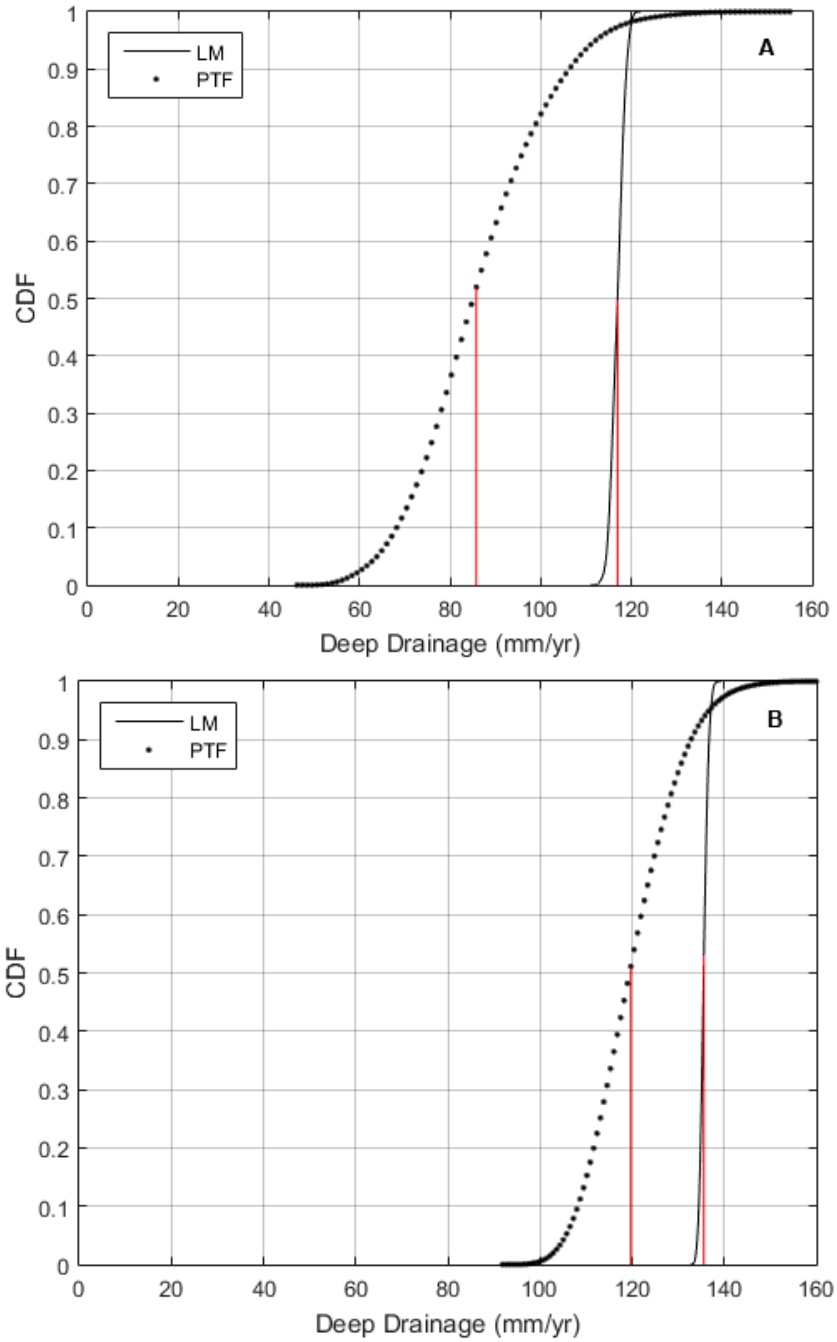

Figure 3.8 Cumulative density function (CDF) for deep drainage under A) pressure head triggered irrigation regime (IR_h) and B) precipitation delayed irrigation regime (IR_{PD}), and two different methods of measuring WRF functions, laboratory measured (LM) and pedotransfer function (PTF). Red lines indicate average deep drainage rates.

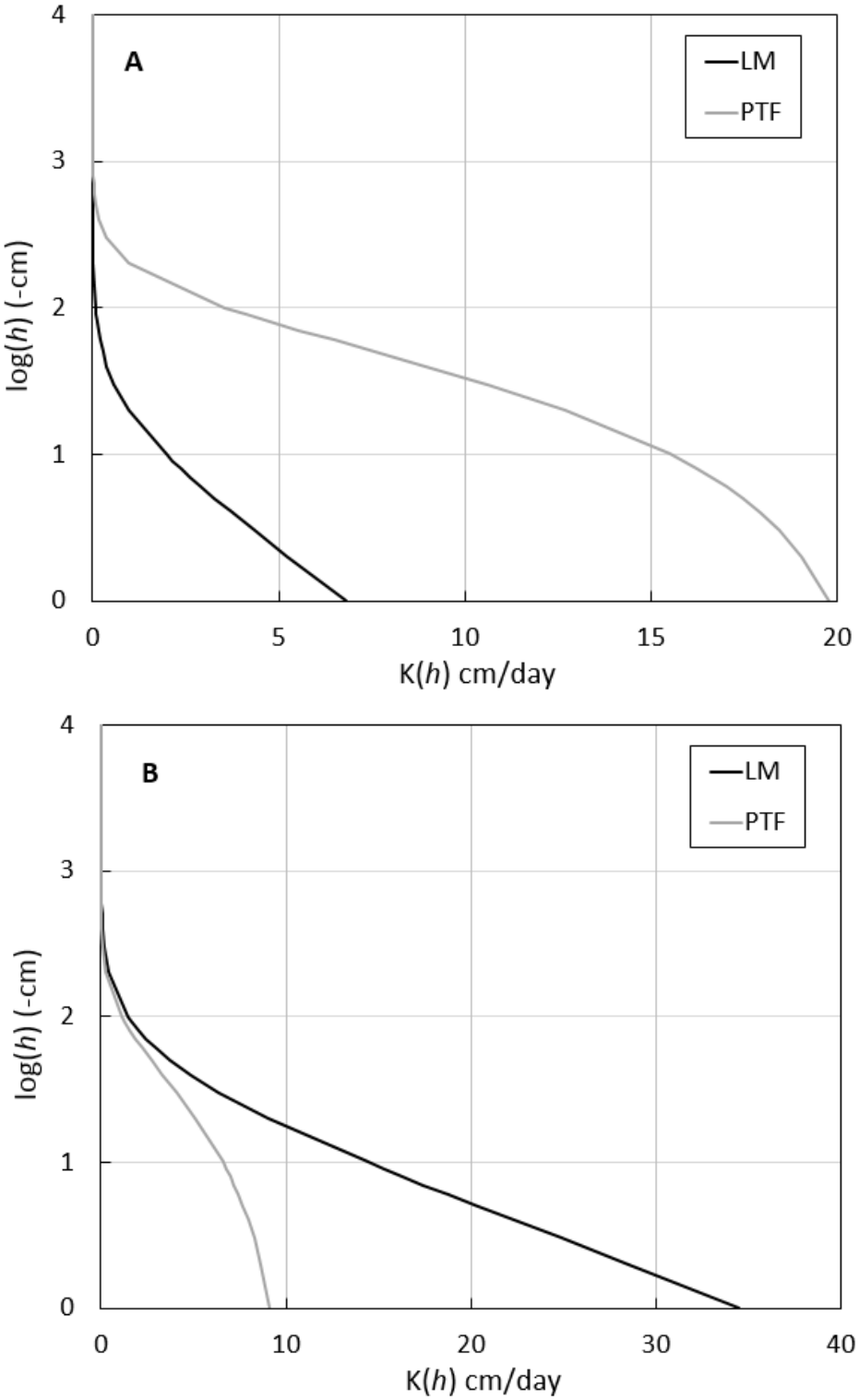

Figure 3.9 Unsaturated hydraulic conductivity (K(*h*)) determined by two methods: laboratory measured (LM) and pedotransfer function (PTF) for the A) upper and B) lower soil layers simulated.

3.3.4.3 Model Parameter Correlation with Deep Drainage Rates

The correlation between each input parameter varied in the uncertainty analysis and 11-year average deep drainage is presented in Figures 3.10 and 3.11. Correlations between each parameter value and deep drainage tended to be low, or linearly related. Table 3.3 contains R^2 and RMSE values for the respective scatter plots.

The relative importance (sensitivity) of certain parameters changed between the two irrigation regimes. Under the IR_h, irrigation is scheduled when the upper portion of the soil profile reaches a certain pressure head. This pressure head is the result of both boundary conditions and soil water properties. Because soil water properties are being varied within the uncertainty analysis, irrigation application varies on a simulation-to-simulation basis. This dynamic irrigation application does not occur within the IR_{PD} – instead irrigation is fixed and based on the frequency of precipitation, which doesn't change from simulation to simulation.

It was also determined that the relative importance of certain parameters also varies within the same irrigation regime but between methods used to determine the WRF. The *n* parameter is the most sensitive parameter for the LM WRF and the α parameter is the most sensitive parameter for the PTF WRF. How each of these parameters impacted deep drainage rates will be discussed in the following sections.

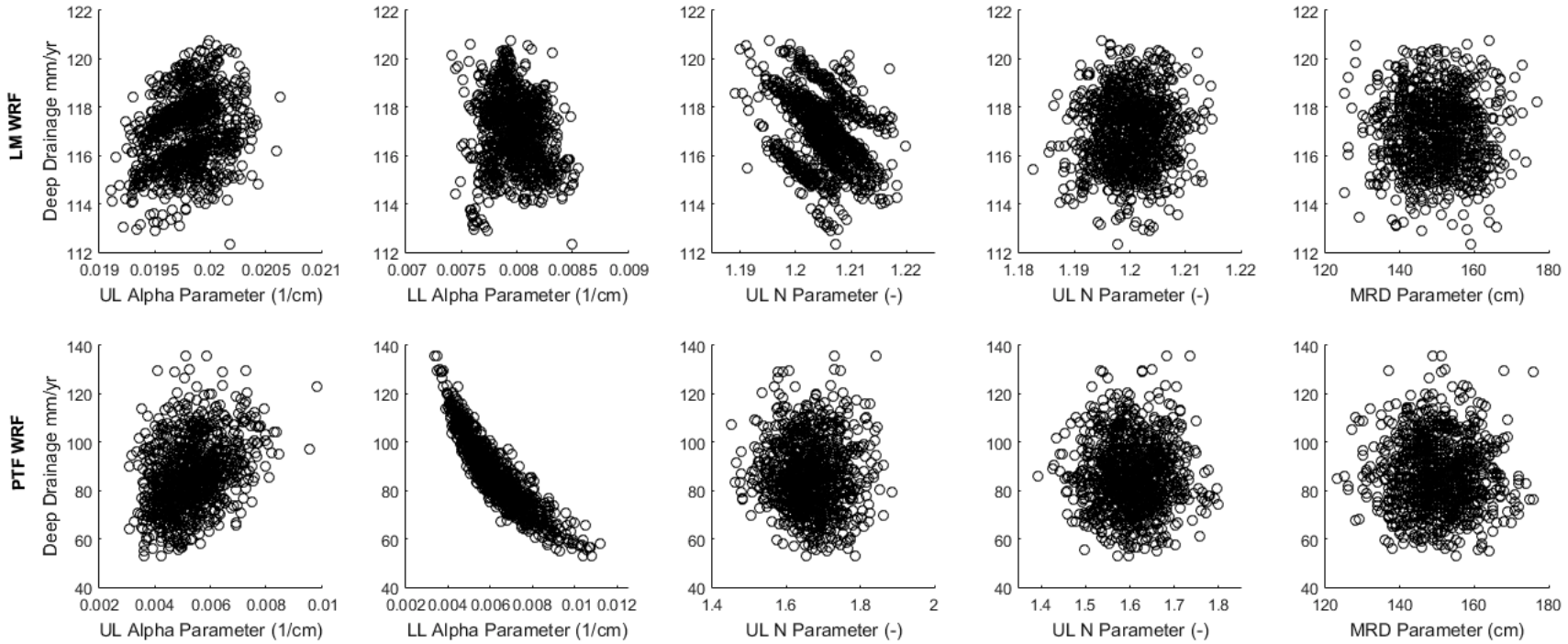

Figure 3.10: Correlation between each parameter and 11-year average drainage within the pressure head triggered irrigation regime (IR_h). The top row presents the laboratory measured (LM) WRF parameters and the bottom row presents the pedotransfer function (PTF) WRF parameters.

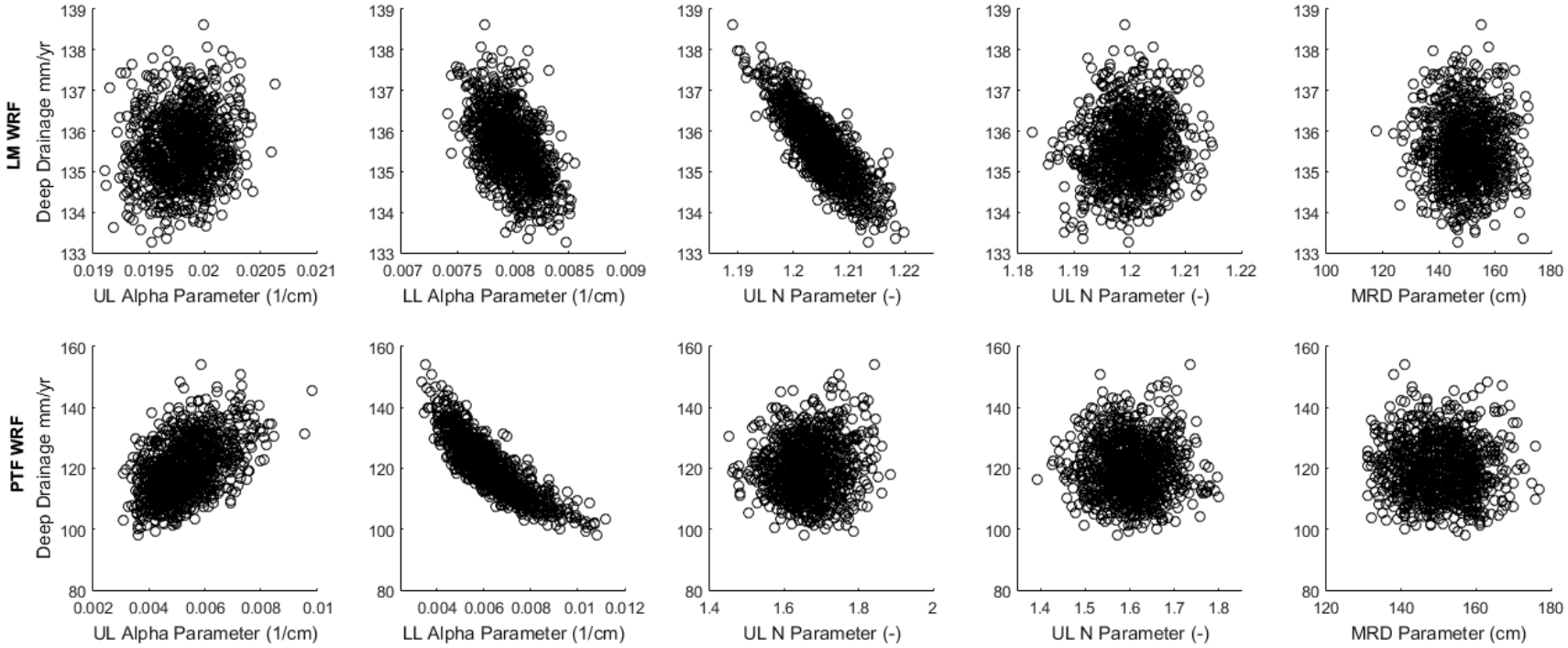

Figure 3.11: Correlation between each parameter and 11-year average deep drainage within the precipitation delayed irrigation regime (IR_{PD}). The top row presents the laboratory measured (LM) WRF parameters and the bottom row presents the pedotransfer function (PTF) WRF parameters.

Table 3.3: R^2 and RMSE values for each parameter vs. 11-year average deep drainage rates.

		Parameter Value vs. Average Annual Deep Drainage		
Irrigation Regime	**Water Retention Function Measurement Method**	**Parameter**	**R^2**	**RMSE (cm)**
Pressure Head Triggered (IR_h)	Laboratory Measured	α Upper Layer	0.076	0.144
		α Lower Layer	0.027	0.147
		n Upper Layer	0.115	0.140
		n Lower Layer	0.005	0.149
		MRD	0.000	0.149
	Pedotransfer Correlation	α Upper Layer	0.121	1.335
		α Lower Layer	0.810	0.620
		n Upper Layer	0.001	1.422
		n Lower Layer	0.000	1.422
		MRD	0.000	1.422
Precipitation Delayed (IR_{PD})	Laboratory Measured	α Upper Layer	0.016	0.083
		α Lower Layer	0.263	0.072
		n Upper Layer	0.686	0.047
		n Lower Layer	0.016	0.083
		MRD	0.001	0.084
	Pedotransfer Correlation	α Upper Layer	0.227	0.801
		α Lower Layer	0.721	0.471
		n Upper Layer	0.008	0.896
		n Lower Layer	0.000	0.897
		MRD	0.001	0.895

3.3.4.4 Parameter α

Of the three potential sources of error, α demonstrated significant sensitivity through all irrigation regimes and both WRF methods (Table 3.3). The α parameter impacts the pressure head (h) of a soil for a given volumetric water content (θ) as seen in the following equations from van Genuchten, 1980:

$$h(S_e) = \frac{1}{\alpha}\left(\frac{1 - S_e^{1/m}}{S_e^{1/m}}\right)^{1/n}, \; m = 1 - 1/n \tag{15}$$

$$S_e = \frac{\theta - \theta_r}{\theta_s - \theta_r} \tag{16}$$

where S_e is volumetric water content, θ, scaled between residual water content, θ_r, and saturated water content, θ_s. A low α parameter value will lead to a low h as seen in Figure 3.12 and vice versa for a high α parameter.

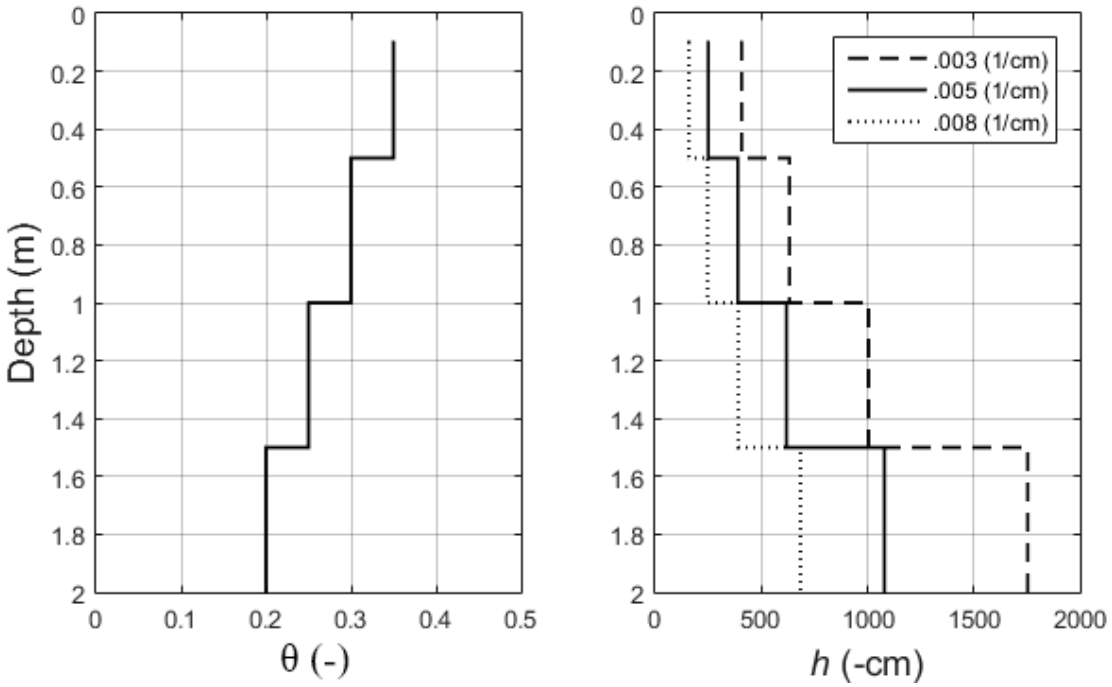

Figure 3.12: Hypothetical moisture profile (θ) and corresponding pressure head profile (h). With different α values (.003, .005, and .008 (1/cm)), the same water content leads to

different pressure head values. The three α values used in this example represent the approximate error range of values for the UL PTF WRF.

In the case of the IR_h, a change in the α parameter may change irrigation application amounts due to shifting the soil profile pressure head closer or further from the irrigation trigger point (set to -1000 cm). In the case of the PTF WRF, α was not well constrained when compared to the LM WRF. Because the irrigation trigger point was held constant (-1000cm), a wide range of irrigation application occurred. This range of irrigation application contributed to the range of deep drainage rates simulated (Figure 3.13).

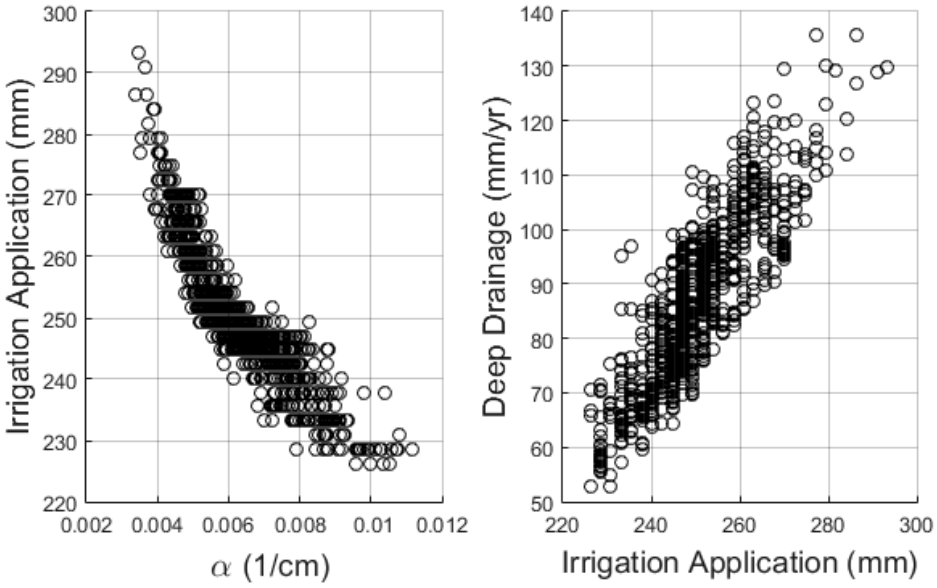

Figure 3.13: Correlation between the α parameter for the lower soil layer, average simulated irrigation application, and resulting average deep drainage as simulated under the IR_h with a water retention function determined via pedotransfer function.

The α parameter also impacts the value of unsaturated hydraulic conductivity (K(h)) for a given head value. This can be seen in Equation 6 and is illustrated in Figure 3.14. The lower the α parameter value, the more conductive the soil profile is for a given head value. This increased conductivity in turn increases deep drainage potential of a

given soil. This can be seen in Figures 3.10-3.11 where an increase in the α parameter decreases average deep drainage.

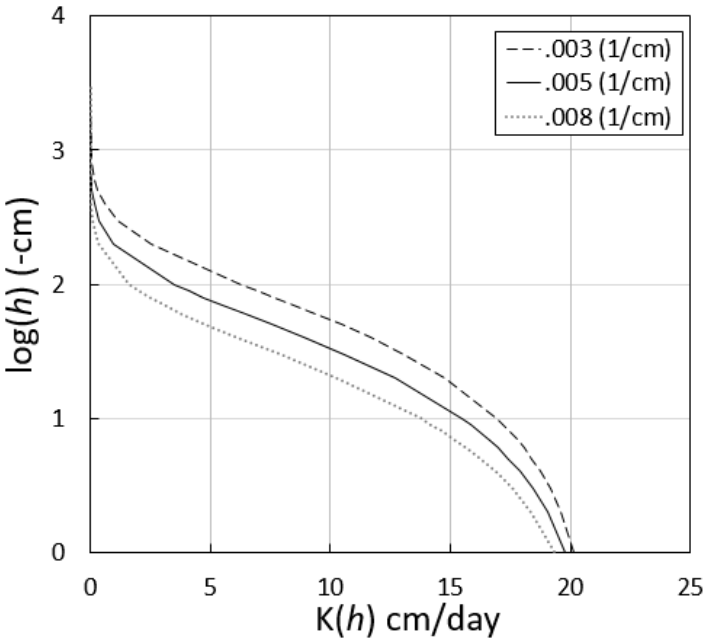

Figure 3.14: With different α values, K(h) has a wide range for a given pressure head (h). The three α values used in this example (.003, .005, .008 (1/cm)) represent the error range of α determined for the UL soil material via PTF.

3.3.4.5 Parameter n

In general, the *n* parameter proved to be relatively insensitive. For the LM WRF, it was the most sensitive parameter selected, but given the small range of deep drainage values, <10 mm/yr, it does not appear to be an important error source. For both WRFs the UL *n* parameter demonstrated a greater sensitivity (higher R^2 value) then the corresponding LL *n* parameter. As can be seen in Figure 3.15, the sensitivity of the n parameter increases as *h* decreases. The more shallow depths in the soil profile experienced greater ranges (wet and dry) of *h* than the lower depths. This explains why the *n* parameter was more important in the UL than the LL.

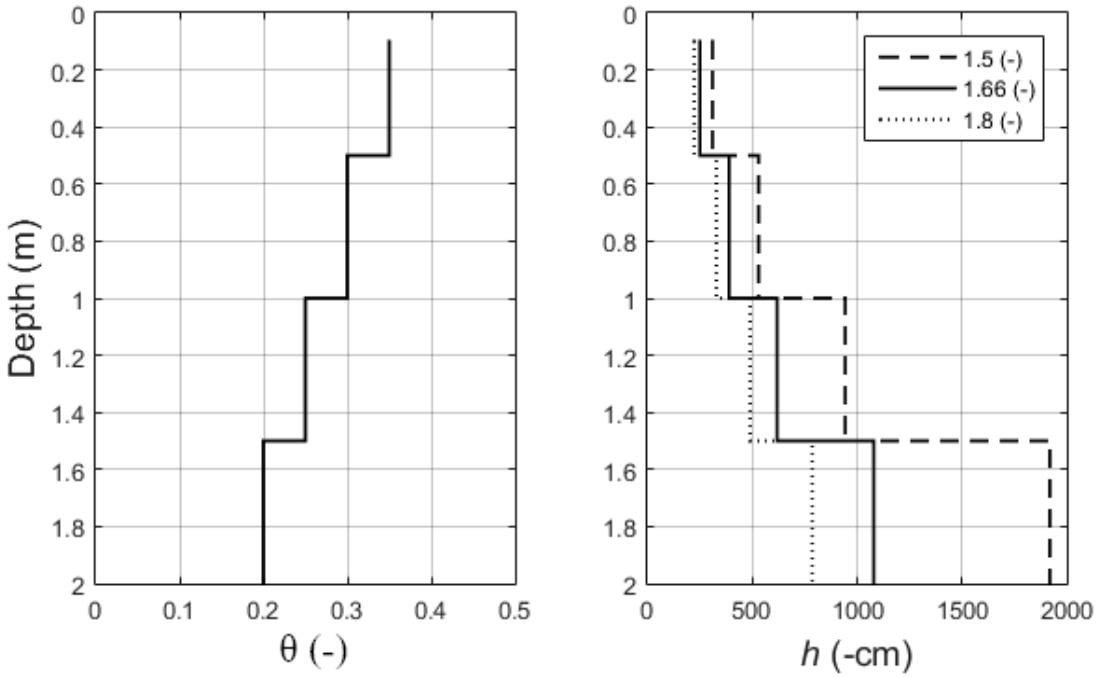

Figure 3.15: Hypothetical moisture profile (θ) and corresponding pressure head (*h*) profile. With different *n* values (1.5, 1.66, and 1.8 (-)), the same water content leads to different pressure head values. In the wet range, this is not a significant effect. The three *n* values used in this example represent the approximate error range of values for the UL PTF WRF.

3.3.4.6 Maximum Rooting Depth Parameter

Within the uncertainty analysis, the *MRD* parameter proved to be insensitive. This is likely due to the following three reasons. Firstly, the primary amount of deep drainage was occurring in the springtime. This is a period of time when root water uptake is low or not occurring as crop emergence has not occurred yet. Secondly, the greater the *MRD* the greater the depth that root water uptake is spread over. As this depth is increased, soil-water depletion over the root zone is mitigated. This mitigation allows roots to better avoid water stress when compared to a shallower root zone. Because the profiles were adequately irrigated, significant water stress was avoided and therefore reduced this effect as regardless of the *MRD*, parameter, root water uptake proceeded at atmospheric

demand. Thirdly, as infiltrated water is percolating downwards, deeper root zones are in contact with percolating water for a longer period of time when compared to shorter root zones. Shorter root zones will have comparatively less time to take up water before percolating water moves past the bottom of the root zone, becoming deep drainage. However, during the growing season, very little downward flux was occurring at the base of the root zone regardless of the possible value of the *MRD* parameter.

3.4 Summary and Conclusions

Results of the modeling indicate that deep drainage in both fields is primarily occurring in the spring. This is a period of time where precipitation is frequent, soil profiles are wet, and ET_p is low. Following the growing season, the till profile tends to be more soil-water depleted than the no-till profile and as a result, has less potential for later deep drainage events in the fall. This appears to be the primary mechanism leading to differences in deep drainage rates between the two simulated fields.

Results of the uncertainty analysis show that a significant range of deep drainage rates are possible when using a PTF when compared to a laboratory measured WRF. Deep drainage rates demonstrated significant sensitivity to a soil property parameter used in the van Genuchten equation, α. This parameter in part describes both the unsaturated hydraulic conductivity and the pressure head of a porous media at a given water content. The *n* parameter demonstrated relative sensitivity in the LM WRF. However, ranges of deep drainage were not large, indicating satisfactory performance. The maximum rooting depth parameter did not demonstrate significant sensitivity in any of the error analyses. This is likely due to deep drainage primarily occurring in the spring, when root water uptake is low. It is also a result of root water uptake primarily proceeding under

atmospheric demand – a goal of proper irrigation management. The parameter may play a larger role if water stress was allowed in an irrigation limited or rain fed scenario.

The discussed H1D simulations were parameterized with both primary field data, and regional data. A significant component of the water balance, ET_c, was estimated from regional weather data and an estimated K_c curve in the case of the no-till filed. Model outputs such as irrigation requirement (specifically in the case of IR_h) agree well with the irrigation data from the in-field flow meter, and deep drainage rates agree well with field specific long term estimations (CMB). With this in mind, the water balance appears to be within reason. However factors such as: crop rotations, crop planting dates, LAI dynamics, and estimations of ET_c via regional scale weather data, were addressed in a simplistic manner. All of these factors may impact ET_a rates which in turn may impact deep drainage rates. Considering these factors, deep drainage rates reported from modeling are not intended to be used as an additional deep drainage estimation for work done in Chapter 2, but rather to bracket differences of deep drainage rates (approximately 100 mm/yr) and to understand the mechanisms leading to differences in those deep drainage rates.

Chapter 4: Conclusions

Deep drainage was monitored under two center pivot irrigation sites located in south-central Nebraska during the 2013, and part of the 2014, growing seasons. It was found that deep drainage occurring under a till field is lower than that of a no-till field. Although field monitoring that was conducted in the 2013 growing season indicated the opposite of this trend, it is believed this is the result of significantly different irrigation application between the two experimental fields – stressing the importance of both land management information and long term monitoring. Key findings of the study include:

- Multiple deep drainage estimations are essential for avoiding bias inherent to each method. Short-term physically based field monitoring techniques are susceptible to temporal uncertainty as well as disturbing of soil at installation. Chemical estimation is biased to the quality of land management data (e.g. irrigation application).
- The CMB analysis indicated that input parameter error constraints had a secondary impact on deep drainage rate uncertainty when compared to the effect of spatial heterogeneity or noise introduced by the methods used for analysis (e.g. Geoprobe® extraction). Significant differences in deep drainage rates were calculated via CMB from 3 extracted soil cores within the same field for both tillage practices. This is an important consideration, as frequently deep drainage studies using this method only extract one core per study area.
- Field data indicated that the two experimental fields had different amounts of irrigation application. It is uncertain if the difference in deep drainage was the result

of differences in irrigation application. Within the modeling investigation, the two simulated fields were irrigated identically. This led to even greater differences in deep drainage between the two fields.

- Results of modeling suggests that differences in deep drainage rates between the two tillage practices occur primarily in the fall, but deep drainage occurs primarily in the spring for both fields.
- The sensitivity of deep drainage rates to van Genuchten water retention fitting parameters (specifically α and n) changes between different irrigation application regimes.
- Greater soil hydraulic parameter error associated with the use of a PTF leads to greater deep drainage uncertainty when compared to LM soil hydraulic parameters.
- The maximum rooting depth parameter had little effect on simulated deep drainage rates.

Future research is needed to determine temporal variability of chloride concentration in irrigation water in order to better constrain inputs in the CMB equation. Future work should also be conducted to determine how much variation occurs in chloride plant matter uptake and subsequent harvest export. An improved method of installing soil water sensors that minimizes disturbing of soil is needed if monitoring for a single year is desired.

References

Allen, R.G., L.S. Pereira, D. Raes, and M. Smith. 1998. Crop evapotranspiration - Guidelines for computing crop water requirements - FAO Irrigation and Drainage Paper 56. *FAO, Rome*. 300(9).

Allison, G.B. and M.W. Hughes. 1983. The use of natural tracers as indicators of soil-water movement in a temperate semi-arid region. *Journal of Hydrology*. 60: 157-173.

AmeriFlux Network. 2013. http://ameriflux.ornl.gov/

Arshad, M.A., M. Schnitzer, D. Angers, and J.A. Ripmeester. 1990. Effects of till vs no-till on the quality of soil organic matter. *Soil Biology and Biochemistry*. 22(5): 595-599.

Bennett, W.F., ed. 1993. *Nutrient Deficiencies & Toxicities in Crop Plants*. St. Paul, MN: APS Press. ISBN: 0-89054-151-5.

Bosch-Rubia, G. 2015. Land Use and Water and Soil Management Practices Impacts on Potential Groundwater Recharge in Loess Regions of South Central Nebraska. MS Thesis. University of Nebraska – Lincoln. http://digitalcommons.unl.edu/biosysengdiss/51

Bobier, M.W., KD. Frank, and R.F. Spalding. 1993. Nitrate-N movement in a fine-textured vadose zone. *Journal of Soil and Water Conservation*. 18:1045-1054

Brady, N.C., and R.R. Weil. 2004. Elements of the Nature and Properties of Soils (2nd ed.). Upper Saddle River, NJ: Pearson Education/Prentice Hall. 116-120.

Byre, K.R., J.M. Norman, L. G. Bundy, and S. T. Gower. 2000. Water-Budget Evaluation of Prairie and Maize Ecosystems. *Soil Science Society of America Journal.* 64: 715-724.

CropWatch. 2014. Disk and Field Cultivation. University of Nebraska – Lincoln, Lincoln, NE. https://cropwatch.unl.edu/tillage/disk

Deck, J.H. 2010. Hydraulic conductivity, infiltration, and runoff from no-till and tilled cropland. MS Thesis. University of Nebraska – Lincoln. http://digitalcommons.unl.edu/biosysengdiss/14

Djaman, K. and S. Irmak. 2013. Actual crop evapotranspiration and alfalfa- and grass-reference crop coefficients of maize under full and limited irrigation and rainfed conditions. *Journal of Irrigation and Drainage Engineering*. 139(6): 433–446.

Eisenhauer, D. 2014. Personal Communication

Exner, M.E., A.J. Hirsh, R.F. Spalding. 2014. Nebraska's groundwater legacy: Nitrate contamination beneath irrigated cropland. Water Resources Research. 50(5): 4474-4489.

Gates, J.B., G.V. Steele, P. Nasta, and J. Szilagyi. 2014. Lithologic influences of groundwater recharge through incised glacial till from profile to region scales: Evidence from glaciated Eastern Nebraska. *Water Resources Research*. 50(1): 466-481.

Gates, J. B., B.R. Scanlon, X. Mu, and L. Zhang. 2011. Impacts of soil conservation on groundwater recharge in the semi-arid Loess Plateau, China. *Hydrogeology Journal*. 19(4): 865-875

Gee, G.W., A.L. Ward, T.G. Caldwell, and J.C. Ritter. 2002. A vadose zone water fluxmeter with divergence control. *Water Resources Research*. 38(8): 16-1 – 16-7.

Grassini P., B. Farmaha, K. Boone. 2015. NRD Field Scale Database. Department of Agronomy and Horticulture. University of Nebraska.

Healy, R.W. 2010. *Estimating Groundwater Recharge*. Cambridge, UK: Cambridge University Press. ISBN 978-0-521-86396-4.

HPRCC. 2014. Weather and Climate Data via an Automated Weather Data Network from the NOAA High Plains Climate Center (HPRCC). High Plains Regional Climate Center, University of Nebraska-Lincoln, Lincoln, NE. http://www.hprcc.unl.edu/awdn/

ICS-2000 Ion Chromatography System. 2006. Dionex Corporation, Sunnyvale, CA.

Irmak, S., 2014 Personal Communication

Irmak, S., J.O. Payero, B. VanDeWalle, J. Rees, and G. Zoubek. 2014. Principles and operational characteristics of watermark granular matrix sensor to measure soil water status and its practical applications for irrigation management in various soil textures. *University of Nebraska Extension Publications*. EC783. http://ianrpubs.unl.edu/live/ec783/build/ec783.pdf

Katupitiya, A., D.E. Eisenhauer, R.B. Ferguson, R.F. Spalding, F.W. Roeth, and M.W. Bobier. 1997. Transactions of the ASABE. 40:1321-1327

Klocke, N.L., D.G. Watts, J.P. Schneekloth, D.R. Davison, R.W. Todd, and A.M. Parkhurst. 1999. Nitrate leaching in irrigated Corn and soybean in semi-arid climate. *Transactions of the ASABE.* 42(6): 1621-1630. http://elibrary.asabe.org/abstract.asp??JID=3&AID=13328&CID=t1999&v=42&i=6&T=1

Klocke, N., R. Currie, and R. Aiken. 2009. Soil water evaporation and crop residues. *Transactions of ASABE*. 52(1):103-110.

Liao, L., C.T. Green, B.A. Bekins, and J.K. Bohlke. 2012. Factors controlling nitrate fluxes in groundwater in agricultural areas. *Water Resources Research*. 48(6).

Lin, D., M. Jin, X. Liang, and H. Zhan. 2013. Estimating groundwater recharge beneath irrigated farmland using environmental tracers fluoride, chloride and sulfate. *Hydrogeology Journal*. 21(7): 1469-1480.

Murdoch, L. 2015. Paper in Review, *Water Resources Research*.

National Atmospheric Deposition Program (NRSP-3). 2014. NADP Program Office, Illinois State Water Survey, Champaign, IL. http://nadp.isws.illinois.edu/

Odhiambo, L.O. and S. Irmak. 2012. Evaluation of the impact of surface residue cover on single and dual crop coefficient methods for estimating soybean actual evapotranspiration. *Agricultural Water Management*. 104:221-234.

Pertassek, T., A. Peters, and W. Durner. 2015. HYPROP-FIT Software User's Manual (v.3.0). UMS GmbH, München, Germany.

Radcliffe, D. and J. Šimůnek. 2010. *Soil Physics with HYDRUS: Modeling and Applications*. Boca Raton, FL: CRC Press, Taylor & Francis Group. ISBN: 978-1-4200-7380-5.

Scanlon, B. R., R.C. Reedy, R.L. Baumhardt, and G. Strassberg. 2008. Impact of deep plowing on groundwater recharge in a semiarid region: Case study, High Plains, Texas. *Water Resources Research*. 44(7).

Schaap, M.G., F.J. Leij, and M.T. van Genuchten. 2001. ROSETTA: A computer program for estimating soil hydraulic parameters with hierarchical pedotransfer functions. *Journal of Hydrology* 250(3): 163-176.

Šimůnek, J., M. Šejna, H. Saito, M. Sakai, and M. Th. van Genuchten. 2013. The HYDRUS-1D Software Package for Simulating the One-Dimensional Movement of Water, Heat, and Multiple Solutes in Variably-Saturated Media (v.4.17). Dept. of Environmental Sciences, University of California Riverside, Riverside, CA.

Sharma, V. and S. Irmak. 2012. Mapping spatially-interpolated precipitation, reference evapotranspiration, actual crop evapotranspiration, and net irrigation requirements: Part II. Actual crop evapotranspiration and net irrigation requirements. *Transactions of the ASABE*. 55(3): 923-936.

Sophocleous, M. 2005. Groundwater recharge and sustainability in the High Plains aquifer in Kansas, USA. *Hydrogeology Journal*. 13(2): 351-365.

Spalding, R.F., D.G. Watts, J.S. Schepers, M.E. Burbach, M.E. Exner, R.J. Poreda, G.E. Martin. 2001. Controlling nitrate leaching in irrigated agriculture. *Journal of Environmental Quality*. 30(4): 1184-1194.

Szilagyi, J., V. Zlotnik, J. Gates, J. Jozsa, 2011. Mapping mean annual groundwater recharge in the Nebraska Sand Hills, USA. Hydrogeology Journal. 19(8): 1503-1513.

Szilagyi, J. and J. Jozsa. 2013. MODIS-aided statewide net groundwater-recharge estimation in Nebraska. *Groundwater*. 51(5): 735-744.

USDA (United States Department of Agriculture). 2014. Farm and Ranch Irrigation Survey (2013). 2012 Census of Agriculture. Document AC-12-SS-1. http://www.agcensus.usda.gov/Publications/2012/Online_Resources/Farm_and_Ranch_Irrigation_Survey/fris13.pdf

USGS (United States Geological Society). 2005. Water use, by category of use, in Nebraska, 2005. Nebraska Water Science Center. [May 2013, March 2015]. http://ne.water.usgs.gov/infodata/wateruse/waterusecategory.html

van Genuchten, M.Th. 1980. A closed-form equation for predicting the hydraulic conductivity of unsaturated soils. *Soil Science Society of America Journal*. 44(5): 892-898.

Wang, T., V.A. Zlotnik, J. Šimůnek, and M.G. Schaap. 2009. Using pedotransfer functions in vadose zone models for estimating groundwater recharge. *Water Resources Research*. 45(1).

Ward, R.C. 2010. There is More Than NPK [PDF presentation document]. Ward Laboratories, Kearney, NE. http://www.wardlab.com/WardUpdates/NTNPK.pdf

Yang, H.S., A. Dobermann, K.G. Cassman, D.T. Walters, and P. Grassini. 2013. Hybrid-Maize (v.2013.4). A simulation model for corn growth and yield. Nebraska Cooperative Extension, University of Nebraska – Lincoln, Lincoln, NE.

Yonts, C.D., S.R. Melvin, D.E. Eisenhauer. 2008. Predicting the Last Irrigation of the Season. *University of Nebraska Extension Publications*. G1871. http://www.ianrpubs.unl.edu/live/g1871/build/g1871.pdf

Young, A.R., M.E. Burbach, and L.M. Howard. 2013. Nebraska Statewide Groundwater-Level Monitoring Report. *Nebraska Water Survey Paper Number 81*. Conservation and Survey Division, University of Nebraska – Lincoln, Lincoln, NE. http://nlcs1.nlc.state.ne.us/epubs/U2375/B002.0081-2013.pdf

Appendix A: Monte Carlo Uncertainty Analysis

In Chapters 2 and 3, uncertainty analyses were carried out via a Monte Carlo (MC) probabilistic uncertainty analysis. The MC analyses discussed were set up in different ways but had the same general framework:

- Possible values of inputs for equations or models were constrained based on either known measurement error, known statistical correlation error, or observation.
- Inputs were randomly selected based on their known probability distribution.
- The equation or model was carried out.
- This process was repeated numerous times.
- Once the probability density functions of outputs (deep drainage) converged in a satisfactory manner the process was stopped.

The method is probabilistic in nature as input variables are randomly selected from known distributions, and therefore outputs are dependent on the probability of each input variable being selected. Because distributions of outputs around mean values can be determined via MC, they are advantageous to simple uncertainty analysis where only low, mean, and high outputs are determined. This is because maximum and minimum ranges of output estimates can be high, but the probability may be low for the respective input combination to occur.

Appendix B: Geophysical Survey: No-till field

In order to help understand the magnitude of spatial variability within the area of the field the 3 cores were extracted from, a geophysical survey was carried out in the no-till field. This survey was conducted on April 21st, 2014, via a DUALEM-21 EMI device. The device measures soil electrical conductivity (mS/m) in a 3 m radius via electromagnetic induction (EMI).

The EMI device was paired with a GPS receiver and was carried through each row of the field in an approximate 1 ha square centered on the location of previous core extraction. Measurements were taken every 1 sec where GPS location and electrical conductivity were recorded. A general lack of heterogeneity can be seen in Figure B.1. Higher conductivity values in the center of the survey are likely the result of field instrumentation (e.g. lysimeter divergence tube, extensometer sensors, and soil moisture sensors). Ideally the survey would have been repeated at a dry time of the year to determine the difference between soil texture and moisture, but this was not possible due to time constraints.

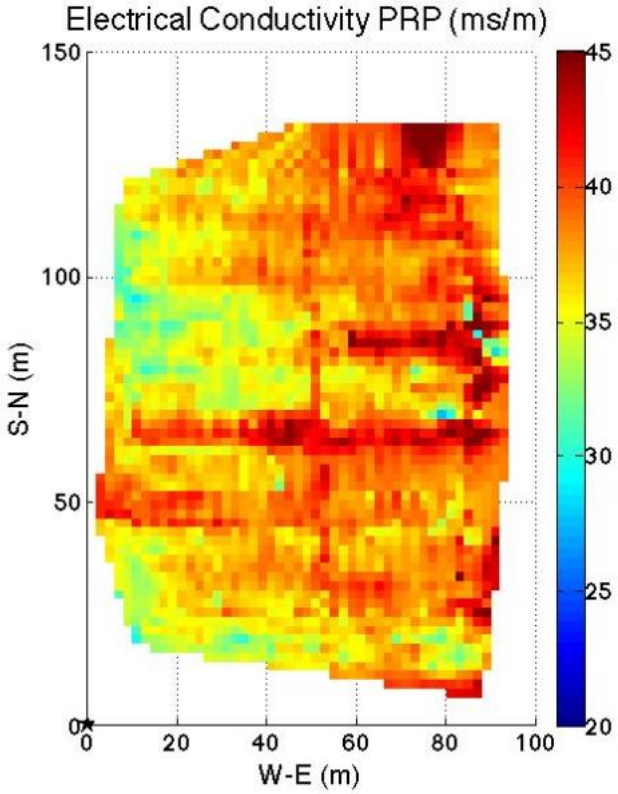

Figure B.1: Geophysical survey conducted on the no-till field in early May 2014. Soil water sensors used in the field monitoring experiment were located in the center of the survey.

Appendix C: Extensometer Sensors

In the no-till field two extensometer sensors were installed within two separate boreholes that reached depths of 12’ and 18’. The purpose of these sensors is to track the strain of the surrounding soil which changes as applied weight (water) is increased (e.g. precipitation and irrigation) or decreased (e.g. deep drainage, runoff, ET) (Murdoch, 2015). The strain of the soil is determined by measuring the change in displacement of an anchor in contact with soil at the bottom of the borehole and outputting a voltage representing that displacement (Murdoch, 2015). Measurements of displacement were taken every 60 seconds. Time series of both sensors for the 2013 monitoring period can be seen in figure C.1. Incomplete data was the result of initial technical difficulties as well as a solar panel that failed to charge the data logger battery. An increase in the signal can be seen in both sensors over time. This is believed to be a seasonal temperature effect and is corrected by fitting a line through the data and subtracting the fitted line value from the measurement value (Murdoch, 2015). The corrected time series can be seen in figure C.2.

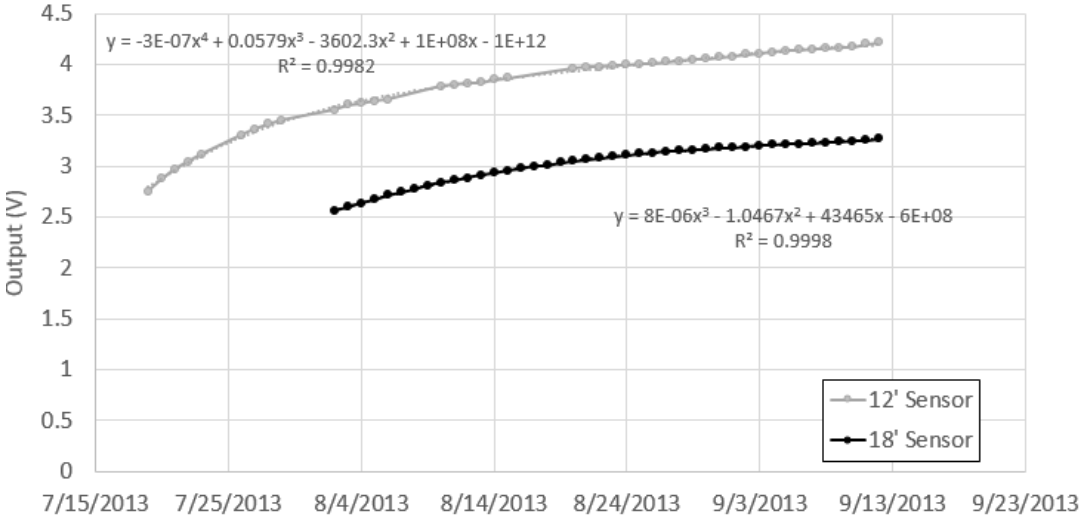

Figure C.1: Average daily outputs from the extensometer sensors in the no-till field. Lines fit through the data represent a temperature effect.

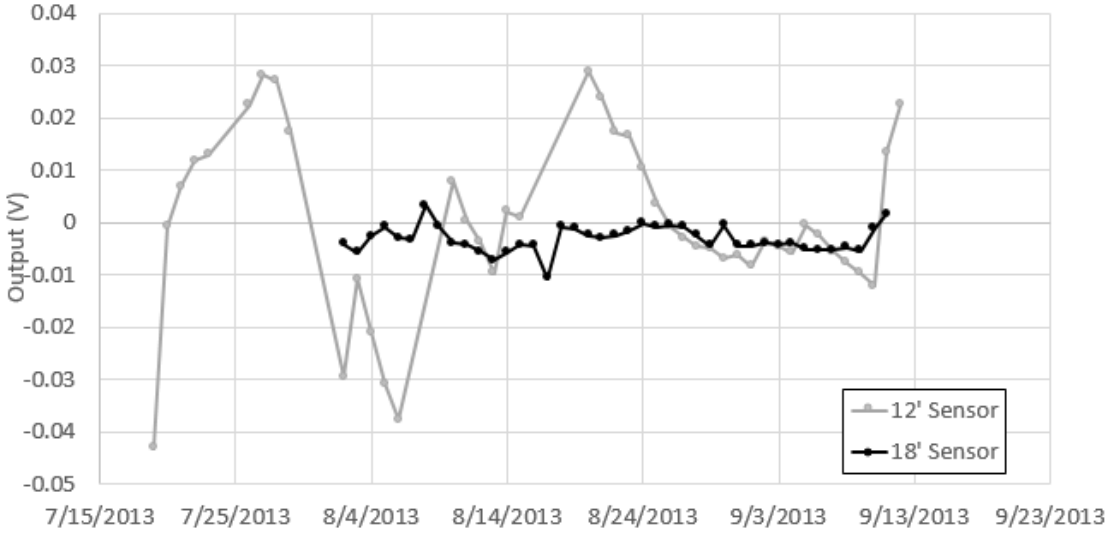

Figure C.2: Corrected average daily outputs from the extensometer sensors in the no-till field.

In the no-till field only two deep drainage events were captured with the installed lysimeter during the period of time when the extensometer sensors were logging data. Due to data gaps in the 12' sensor, it is not possible to estimate the magnitude of these deep drainage events with this sensor. Figure A1.3 focuses on the timeframe when the deep drainage events occurred and for the 18' sensor only. When looking at Figure C.3, comparison of the periods of time when deep drainage indicated by the lysimeter occurred (T2 and T5 on Figure C.3) with the extensometer signal, it appears that there was good agreement between both sensors. Deep drainage from this method can be estimated from the following equation:

$$DD = P\frac{VR_{DD}}{VR_P} \tag{17}$$

where DD is deep drainage in mm, P is a precipitation event in mm, VR_{DD} is the voltage response of the extensometer, and VR_P is the voltage response of a given rain event. Following this method, the first deep drainage event is 4 mm, and the second event is 7

mm. The total of those estimates are approximately 45% of what the lysimeter measured, which was 15 mm and 9 mm for the first and second events respectively. It is uncertain why the two methods did not compare well in magnitude, but the extensometer method is still under development. This could be due to precipitation measurements from a weather station 3 miles away. Field-to-field rain variability may explain poor performance stemming from a poor calibration of the signal response – stressing the importance of an in-field rain gauge. The timing of the signals between the lysimeter and the extensometer did however compare very well. The response of the extensometer does seem to be logical, it can be seen when then center pivot approaches the sensor and registers a sharp peak in the voltage indicating irrigation application and the weight of the pivot arm. Then as the pivot lateral moves away, voltage returns close to is initial value. After some delay, a drainage event increases voltage and this aligns well with the lysimeter drainage time series. In general, more field data and deep drainage events are needed to understand the drainage dynamics of this method, as well as both sensors capturing the drainage events at different depths.

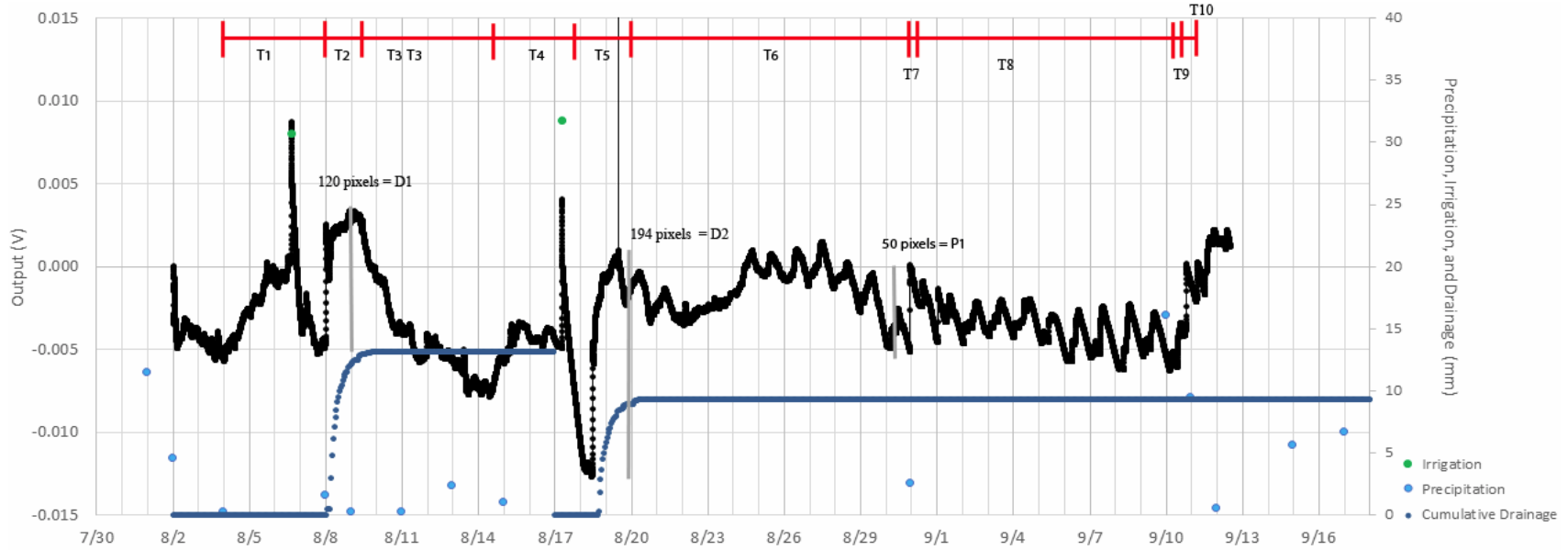

Figure C.3: Annotated extensometer time series for the 18' extensometer with overlain cumulative deep drainage from a nearby lysimeter.

T1: Center Pivot is approaching the sensor and voltage is slowing increasing. The peak represents when the pivot lateral actually arrives.
T2: After the pivot has moved past and a short delay, drainage picks up rapidly.
T3: Voltage is slowly decreasing due to ET and possible drainage not picked up by lysimeter.
T4: Pivot lateral is again approaching the sensor, the peak occurs when the lateral is over the sensor.
T5: Again, after the pivot has fully moved past/a short delay, drainage picks up rapidly.
T6: Diurnal oscillations likely caused by barometric fluctuations.
T7: Rain event occurs and voltage increases.
T8: Diurnal oscillations likely caused by barometric fluctuations.
T9: Another rain event with an upward response.
T10: End of monitoring.

Appendix D: Estimating Evapotranspiration for the No-till Field

Estimating crop specific potential evapotranspiraiton (ET_c) for the no-till field was necessary in order to provide a reasonable ET_p dynamic as an input in the vadose zone model when simulating deep drainage in Chapter 3. A popular approach to estimate ET_c is presented in FAO 56, 1998 and was breifly outlined in Chapter 3.2.3. In addition to a refrence crop potential evapotranspiraton, this method requires predetermined crop coeffiencts (K_c) of which encompass crop development as well as the average effect of soil on evaporation rates. Because no-till fields have a reduction of evaporation due to surface residue (Klocke et al., 2009; Odhiambo and Irmak, 2012), generic K_c coefficients published for corn are not representative and likely would overestimate ET_c. Due to a lack of available K_c coefficients for no-till corn, these coefficients were estimated from data collected at an Ameriflux no-till research site located in Mead, NE (Ameriflux, 2013).

Actual evapotranspiration data for the years 2009-2012 was obtained from the Ameriflux data set for the no-till field. Daily crop coefficients for the 2009 and 2010 growing seasons were determined as:

$$K_c = \frac{ET_a}{ET_{NE}} \tag{18}$$

where, ET_a is daily actual evapotranspiration, ET_{NE} is a reference ET_p, and K_c is a dimensionless coefficient. ET_a was measured by an in-field eddy covariance tower and ET_{NE} was determined from a nearby HPRCC weather station (HPRCC, 2014). K_c values were averaged over every 100 GDD (^oC) for both seasons. A 3rd order polynomial was then

fit through the averaged K_c values for both seasons as described in Djaman and Irmak, 2013. The fit of this curve through both seasons was determined to be reasonable (R^2 of .891) and was used as the K_c curve.

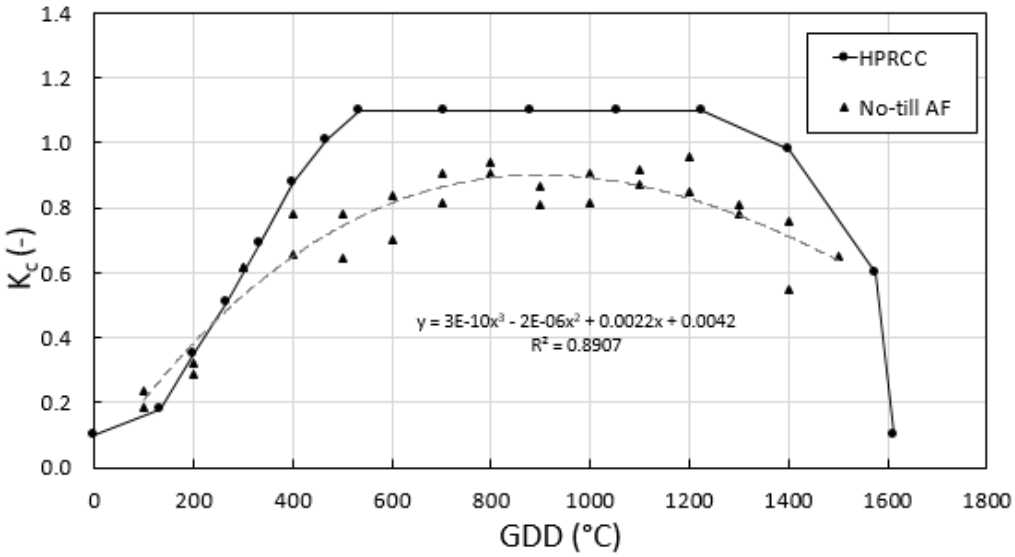

Figure D.1: K_c curve calculated from measured ET_a data at a no-till center pivot irrigation Ameriflux (AF) research site in Mead, NE, and HPRCC published K_c coefficients for corn plotted for reference.

The performance of this curve was tested by estimating the ET_c for the 2011 and 2012 years. This time series can be seen in Figure D.2. In 2011 the total seasonal estimated ET_a was 13% lower than what was measured. In 2012 the total seasonal estimated ET_a was 13% higher than what was measured. Considering the relative closeness of measured and predicted values, along with a lack of bias indicated by the 2 calibration years, the performance of this K_c curve was determined to be satisfactory for the Mead, NE, research site.

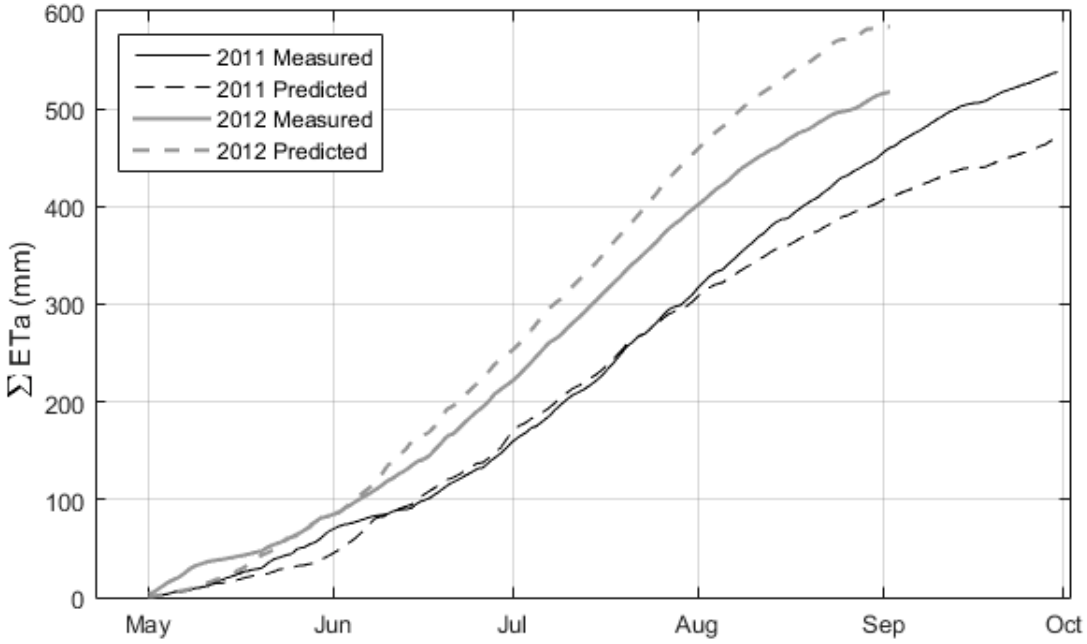

Figure D.2: Time series comparison of cumulative measured and predicted ET_a for the Ameriflux Mead, NE, no-till research site.

It is uncertain what the performance of this curve is when applied to the Holdrege, NE area as outlined in Chapter 3. An oversimplified water balance calculated from field data presented in Chapter 2 is as follows:

$$ET_a = P + I - DD \tag{19}$$

where ET_a is annual average actual evapotranspiration (mm/yr), P is annual average precipitation (mm/yr), I is annual average irrigation (mm/yr), and DD is annual average deep drainage (mm/yr). This approach does not consider potential runoff, or run-on, but is the best field-specific data available. For the no-till field, using the 5 year average for P+I of 730 mm/yr, and the 5 year average CMB estimate of 210 mm/yr for deep drainage, ET_a would be approximately 520 mm/yr. Results of the H1D simulations using this K_c curve indicate an ET_a of 530 mm/yr suggesting the magnitude of the ET_a dynamic is within reason.